Journal of Fluids and Structures (1999) **13,** 75–101
Article No.: jfls. 1998.0190
All articles available online at http://www.idealibrary.com on IDEAL

FLUTTER OF AN AIRFOIL WITH A CUBIC RESTORING FORCE

B. H. K. Lee, L. Y. Jiang

Institute for Aerospace Research, National Research Council
Ottawa, Ontario, K1A 0R6, Canada

AND

Y. S. Wong

Department of Mathematical Sciences, University of Alberta
Edmonton, Alberta, T6G 2G1, Canada

(Received 23 February 1998 and in revised form 8 September 1998)

In this paper, the effect of a cubic structural restoring force on the flutter characteristics of a two-dimensional airfoil placed in an incompressible flow is investigated. The aeroelastic equations of motion are written as a system of eight first-order ordinary differential equations. Given the initial values of plunge and pitch displacements and their velocities, the system of equations is integrated numerically using a fourth order Runge-Kutta scheme. Results for soft and hard springs are presented for a pitch degree-of-freedom nonlinearity. The study shows the dependence of the divergence flutter boundary on initial conditions for a soft spring. For a hard spring, the nonlinear flutter boundary is independent of initial conditions for the spring constants considered. The flutter speed is identical to that for a linear spring. Divergent flutter is not encountered, but instead limit-cycle oscillation occurs for velocities greater than the flutter speed. The behaviour of the airfoil is also analysed using analytical techniques developed for nonlinear dynamical systems. The Hopf bifurcation point is determined analytically and the amplitude of the limit-cycle oscillation in post-Hopf bifurcation for a hard spring is predicted using an asymptotic theory. The frequency of the limit-cycle oscillation is estimated from an approximate method. Comparisons with numerical simulations are carried out and the accuracy of the approximate method is discussed. The analysis can readily be extended to study limit-cycle oscillation of airfoils with nonlinear polynomial spring forces in both plunge and pitch degrees of freedom.

1. INTRODUCTION

Cubic nonlinearities in one-degree-of-freedom (dof) mechanical and electrical systems can often be represented by a Duffing's equation that has been the subject of investigation for many years. The two classical books by Stoker (1950) and Hayashi (1964) give an excellent account of the behaviour of Duffing's equation and more recent studies by Ueda (1980), Thompson & Stewart (1986) and Dowell & Ilgamov (1988) deal with chaotic characteristics of that well-known equation.

Numerical simulation of Duffing's equation was carried out by Jones & Lec (1985) and they demonstrate the sensitivity to initial conditions in the jump phenomenon. The dynamic response of a coupled 2-dof system with cubic nonlinearities was investigated

0889–9746/99/010075 + 27 $30.00

analytically and numerically by Wong *et al.* (1995), who showed that the amplitude–frequency curve has a much more complex structure compared to a 1-DOF system. The amplitude–frequency relation changes from a cubic equation for a 1-DOF system to a polynomial of degree nine for a 2-DOF system. The coupled Duffing's equations were further investigated by Gong *et al.* (1998), who showed that harmoic, quasi-periodic and chaotic motions can exist for system parameters that correspond to those commonly used to analyse aeroelastic behaviour of aircraft structures. In fact, the equations studied by Wong *et al.* (1995) and Gong *et al.* (1998) were derived for an airfoil performing pitch and plunge motions but with the aerodynamic terms neglected. The intention of those investigations dealing with purely mechanical systems was to understand the dynamics of coupled Duffing's equations before introducing further complexities when aerodynamic forces are included.

The first attempt to study the effects of a cubic structural nonlinearity in aeroelasticity was carried out by Woolston *et al.* (1955, 1957) using an analog computer. They analysed a 2-DOF system for hard and soft springs in the torsional degree of freedom of a pitch and plunge system. A hard spring can be used to represent a thin wing or a propeller blade subjected to increasing amplitudes of torsion, while a soft spring may be associated with panel buckling. The spring stiffness was represented by the sum of a linear and a cubic term. Results were given in the form of plots of initial angular displacement versus flutter velocity. For a hard spring, the flutter boundary is a straight line at the flutter speed of the linear system. The soft spring has a destabilizing effect, in that flutter could be induced below the linear flutter speed by making the initial displacement sufficiently large. For both linear and soft springs, the flutter was divergent at any velocity above the flutter boundary. However, for a hard spring, the flutter amplitude is self-limited. The limit amplitude is a function of velocity, and it increases as velocity is increased beyond the flutter boundary.

In other configurations, cases have been found where a hard spring can be destabilizing, and it appears that effects produced by a cubic spring depend on the stiffness of the linear term. Generally, flutter speed decreases as the bending–torsion frequency ratio approaches unity. If a cubic spring, whether soft or hard, tends to make this ratio approach unity, it will probably have a destabilizing effect. Woolsen *et al.* (1955, 1957) made these concluding remarks in their paper without actually showing any results.

Lee & LeBlanc (1986) analysed numerically 2-DOF airfoil motion with a cubic nonlinearity in the pitch degree of freedom. They investigated the effects of initial pitch displacement on the flutter boundaries of soft and hard springs, as well as the amplitudes of pitch and plunge motion of limit-cycle oscillations for various system parameters. Houbolt's (1950) implicit finite-difference scheme was employed throughout their study. Using incompressible aerodynamics, the aeroelastic equations for a two-dimensional airfoil performing plunge and pitch motions were written as a pair of simultaneous finite-difference equations. Their conclusions agreed with the limited results given by Woolston *et al.* (1955, 1957) on the behaviour of the flutter boundaries for soft and hard springs. Lee & LeBlanc (1986) also investigated the effects of airfoil/air-mass ratio, undamped plunge/pitch natural frequency ratio, distance between elastic axis and centre of mass of airfoil, and various stiffnesses of the nonlinear spring on the airfoil response. In their study, the stiffness nonlinearity is represented by the sum of a linear and a cubic term similar to that given by Woolston *et al.* (1995, 1957). If we write it as $\beta_1\alpha + \beta_3\alpha^3$, where β_1 and β_3 are constants and α is the pitch displacement, the smallest value of β_1/β_3 considered by Lee & LeBlanc (1986) was 0·3333. For pitch angles in the range $\alpha < 15^\circ$, where linear aerodynamics can be used, the cubic stiffness term is small compared with the linear term.

O'Neil *et al.* (1996) performed experiments on the existence of limit-cycle oscillation (LCO) of an airfoil with cubic structural nonlinearities and compared their results with

numerical simulations such as those given by Lee & LeBlanc (1986). They found that the stability boundary is sensitive to initial conditions, and the amplitude and frequency of the airfoil response depend primarily on the freestream velocity.

Price *et al.* (1995) studied cubic nonlinearity using numerical and describing-function techniques. The describing-function technique cannot be used to investigate the effects of initial conditions but gives good predictions of magnitudes of LCO. The airfoil properties chosen were the same as those used by Lee & Desrochers (1987). Two values of the ratio $\beta_1/\beta_3 = 0{\cdot}0025$ and $0{\cdot}0002$ were used. These values indicate that the linear stiffness is small compared to the nonlinear terms for small or moderate pitch angles. In other words, the system is not a perturbation from a linear system as in Lee & LeBlanc (1986) studies. As pointed out by Woolston *et al.* (1955, 1957), a hard spring can be destabilizing depending on the stiffness of the linear term. Chaotic motion was observed from bifurcation diagrams and Poincaré maps. Because of the analytical nature of the cubic nonlinearity, it is possible to calculate the Lyapunov spectrum directly from the differential equations. A small value of $0{\cdot}01$ was computed for a limited range of velocity using Lee & Desrochers' (1987) airfoil parameters and this indicates the system is midly chaotic. The route to chaos is from frequency doubling with increasing velocity. Price *et al.* (1995) concluded that a hard spring gives LCO at velocities well below the divergent flutter boundary. When the LCO is period-one there is good agreement in the amplitude of airfoil motion derived from numerical finite-difference and describing-function solutions. However, the describing function cannot predict higher-order periodic solutions and Johnson's (1952) method can be used to compute the second or higher harmonics.

Zhao & Yang (1990) carried out a similar analysis on a two-dimensional airfoil in incompressible flow with a cubic restoring moment in pitch. They investigated the effect of elastic axis position on the dynamic response of an airfoil. Both a describing function and a time-marching method using the Runge–Kutta numerical scheme were employed. Zhao & Yang (1990) found that chaos would occur for velocities in excess of that required for static divergence. The aerodynamics used was quasi-static where the lift and pitching moment depend only on the instantaneous pitch angle. This difference in aerodynamics from an unsteady analysis using Wagner's function has been pointed out by Price *et al.* (1995) to have a considerable effect on the dynamic response of the airfoil, and more realistic aerodynamics should be used to give a better prediction of the airfoil behaviour.

Poirion (1993) used a normal mode basis approach to describe the nonlinear vibrations of an airfoil. Nonlinear structural elements are replaced with equivalent linear ones and the displacement vector of a point located on the nonlinear structure is represented by the summation of a finite number of terms involving the product of the generalized coordinates and the linearized structure mode shapes. The equations of motion are constructed in the time domain using generalized aerodynamic forces in the form of rational functions of the Laplace variable. Poirion (1993) considered an example of a cubic nonlinear restoring force, and the aircraft structure was modelled using three elastic normal modes with nonlinear restoring force applied to each mode. An implicit scheme was used to solve the equations numerically. The value of β_1/β_3 used is 10 for all three modes and this value makes the cubic term small compared with the linear term. Also, β_1/β_3 is considerably larger than the values used by Price *et al.* (1995) and Zhao & Yang (1990) and chaos is usually not encountered when the nonlinear stiffness term is small compared with the linear term. At an airspeed of $1{\cdot}333$ times the linear flutter speed, the generalized coordinates trajectories exhibit a LCO.

In this paper, the method developed by Wong *et al.* (1995) and Gong *et al.* (1998) for coupled nonlinear mechanical systems is extended to study the dynamic response of an airfoil with soft and hard cubic structural nonlinearities. The aeroelastic equations are formulated as a set of eight first-order ordinary differential equations. This approach allows

existing methods suitable for the study of ordinary differential equations to be used in the analysis. Adopting a fourth-order Runge–Kutta integration scheme, the effects of initial conditions on the flutter boundaries are studies in greater detail than those described in Lee & LeBlanc's (1986) report. Investigation of pre- and post-Hopf-bifurcation is carried out using methods developed for studying stability near equilibrium points of nonlinear oscillating systems. The amplitudes of pitch and plunge motions of LCO for post-Hopf-bifurcation are computed for a hard spring and compared with numerical simulations. Small values of the ratio of cubic to linear structural stiffness are chosen, so that chaos is not encountered in this study.

The numerical results presented in this paper are for a single nonlinearity in the pitch degree of freedom. Examples of coupled cubic nonlinearities in the plunge and pitch motions are not studied since, even in the absence of aerodynamics, the equations of motion describing the coupled Duffing's oscillators show an extremely complex jump condition, as demonstrated by Lee *et al.* (1997). There are a large number of possibilities, and perhaps unknown complexities, of airfoil motion that may occur when various parameters of the nonlinearities are varied. This, together with the fact that a number of variables are needed to define the airfoil, makes a complete parametric study of the simple two-degree-of-freedom system practically impossible. In addition, four initial conditions specifying the plunge and pitch displacements and their time derivatives are required to uniquely define the problem. A systematic study of initial conditions has not been attempted, and in determining the flutter boundary, only one pair of initial conditions (pitch displacement and velocity or plunge displacement and velocity) is varied at a time, while keeping the other pair equal to zero. The examples given in this paper on cubic structural nonlinearities are therefore incomplete, but leave opportunities for the interested reader to explore more complex airfoil motions that can be encountered with various coupled nonlinearities, airfoil parameters and initial conditions.

2. ANALYSIS

2.1. Two-Degree-of-Freedom Airfoil Motion with Cubic Structural Nonlinearities

Figure 1 gives the symbols used in the analysis of a two-degree-of-freedom airfoil oscillating in pitch and plunge. The plunge deflection is denoted by h, positive in the downward direction, and α is the pitch angle about the elastic axis, positive with nose up. The elastic axis is located at a distance $a_h b$ from the mid-chord, while the mass centre is located at a distance $x_\alpha b$ from the elastic axis. Both distances are positive when measured towards the trailing edge of the airfoil. The aeroelastic equations of motion for linear springs have been derived by Fung (1969). For nonlinear restoring forces such as those for cubic springs in both pitch and plunge, they are given by Lee *et al.* (1997) as follows:

$$\xi'' + x_\alpha \alpha'' + 2\zeta_\xi \frac{\bar{\omega}}{U^*}\xi' + \left(\frac{\bar{\omega}}{U^*}\right)^2 (\xi + \beta_\xi \xi^3) = -\frac{1}{\pi\mu} C_l(\tau), \tag{1}$$

$$\frac{x_a}{r_a^2}\xi'' + \alpha'' + 2\frac{\zeta_\alpha}{U^*}\alpha' + \frac{1}{U^{*2}}(\alpha + \beta_\alpha \alpha^3) = \frac{2}{\pi\mu r_a^2} C_{1l}(\tau), \tag{2}$$

where $\xi = h/b$ is the nondimensional plunge displacement of the elastic axis, β_ξ, and β_α are the nonlinear spring constants, r_α is the radius of gyration about the elastic axis, and ζ_ξ and ζ_α are the viscous damping coefficients in plunge and pitch, respectively.

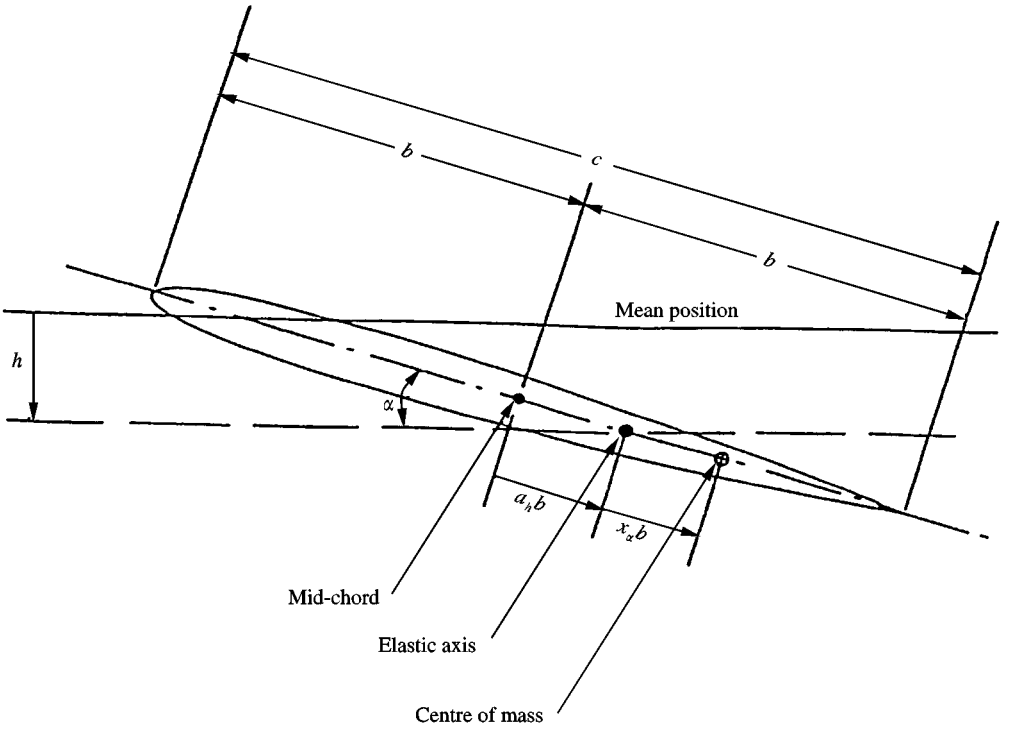

Figure 1. Schematic of a two-degree-of-freedom airfoil motion.

In equations (1) and (2), U^* is defined as

$$U^* = \frac{U}{b\omega_\alpha}, \tag{3}$$

and $\bar{\omega}$ is given by

$$\bar{\omega} = \omega_\xi/\omega_\alpha, \tag{4}$$

where ω_ξ and ω_α are the uncoupled plunging and pitching modes natural frequencies, and the prime denotes the differentiation with respect to the nondimensional time τ defined as

$$\tau = Ut/b. \tag{5}$$

$C_L(\tau)$ and $C_M(\tau)$ in equations (1) and (2) are the lift and pitching moment coefficients, respectively. For incompressible flow, Fung (1969) gives the following expressions for $C_L(\tau)$ and $C_M(\tau)$:

$$C_L(\tau) = \pi(\xi'' - a_h\alpha'' + \alpha') + 2\pi\{\alpha(0) + \xi'(0) + [\tfrac{1}{2} - a_h]\alpha'(0)\}\phi(\tau) + 2\pi\int_0^\tau \phi(\tau-\sigma)[\alpha'(\sigma) + \xi''(\sigma) + [\tfrac{1}{2} - a_h)\alpha''(\sigma)]\,\mathrm{d}\sigma, \tag{6}$$

$$C_M(\tau) = \pi(\tfrac{1}{2} + a_h)\{\alpha(0) + \xi'(0) + (\tfrac{1}{2} - a_h)\alpha'(0)\}\phi(\tau) + \pi(\tfrac{1}{2} + a_h)\int_0^\tau \phi(\tau-\sigma)\{\alpha'(\sigma) + \xi''(\sigma) + (\tfrac{1}{2} - a_h)\alpha''(\sigma)\}\,\mathrm{d}\sigma + \tfrac{\pi}{2}a_h(\xi'' - a_h\alpha'') - (\tfrac{1}{2} - a_h)\tfrac{\pi}{2}\alpha' - \tfrac{\pi}{16}\alpha'', \tag{7}$$

where the Wagner function $\phi(\tau)$ is given by

$$\phi(\tau) = 1 - \Psi_1 e^{-\varepsilon_1 \tau} - \Psi_2 e^{-\varepsilon_2 \tau}, \tag{8}$$

and the constants $\Psi_1 = 0{\cdot}165$, $\Psi_2 = 0{\cdot}335$, $\varepsilon_1 = 0{\cdot}0455$ and $\varepsilon_2 = 0{\cdot}3$ are obtained from Jones (1940).

Due to the existence of the integral terms in the integro-differential equations (1) and (2), it is difficult to study the dynamic behaviour of the system analytically. For example, the system stability near equilibrium points cannot be analysed readily since most of the presently available methods for nonlinear systems are developed for ordinary differential equations. In order to be able to study this system of equations analytically, Lee *et al.* (1997) derived a set of ordinary differential equations by introducing four new variables

$$w_1 = \int_0^\tau e^{-\varepsilon_1(\tau-\sigma)} \alpha(\sigma)\, d\sigma, \quad w_2 = \int_0^\tau e^{-\varepsilon_2(\tau-\sigma)} \alpha(\sigma)\, d\sigma,$$

$$w_3 = \int_0^\tau e^{-\varepsilon_1(\tau-\sigma)} \xi(\sigma)\, d\sigma, \quad w_4 = \int_0^\tau e^{-\varepsilon_2(\tau-\sigma)} \xi(\sigma)\, d\sigma. \tag{9}$$

Equations (1) and (2) can be written as

$$c_0\xi'' + c_1\alpha'' + c_2\xi' + c_3\alpha' + c_4\xi + c_5\xi^3 + c_6\alpha + c_7 w_1 + c_8 w_2 + c_9 w_3 + c_{10} w_4 = f(\tau), \tag{10}$$

$$d_0\xi'' + d_1\alpha'' + d_2\alpha' + d_3\alpha + d_4\alpha^3 + d_3\xi' + d_6\xi + d_7 w_1 + d_8 w_2 + d_9 w_3 + d_{10} w_4 = g(\tau), \tag{11}$$

where the coefficients in equations (10) and (11) are given in Lee *et al.* (1997); $f(\tau)$ and $g(\tau)$ are given by

$$f(\tau) = \frac{2}{\mu}[(\tfrac{1}{2} - a_h)\alpha(0) + \xi(0)]\,(\Psi_1 \varepsilon_1 e^{-\varepsilon_1 \tau} + \Psi_2 \varepsilon_1 e^{-\varepsilon_2 \tau}), \tag{12}$$

and

$$g(\tau) = -\frac{(1 + 2a_h) f(\tau)}{2r_\alpha^2}. \tag{13}$$

After introducing a variable vector $\mathbf{X} = \{x_1, x_2, \ldots, x_8\}^{\mathrm{T}}$ defined as

$$x_1 = \alpha, \quad x_2 = \alpha', \quad x_3 = \xi, \quad x_4 = \xi',$$

$$x_5 = w_1, \quad x_6 = w_2, \quad x_7 = w_3, \quad x_8 = w_4. \tag{14}$$

Equations (10) and (11) can be written as a set of eight first-order ordinary differential equations,

$$\mathbf{X}' = \mathbf{f}(\mathbf{X}; U^*), \tag{15}$$

where the nondimensional velocity U^* is a parameter. In terms of vector components, equation (15) can be expressed as

$$x_1' = x_2, \quad x_2' = (c_0 H - d_0 P)/(d_0 c_1 - c_0 d_1), \quad x_3' = x_4,$$

$$x_4' = (-c_1 H + d_1 P)/(d_0 c_1 - c_0 d), \quad x_5' = x_1 - \varepsilon_1 x_5, \quad x_6' = x_1 - \varepsilon_2 x_6,$$

$$x_7' = x_3 - \varepsilon_1 x_7, \quad x_8' = x_3 - \varepsilon_2 x_8, \tag{16}$$

where

$$P = c_2 x_4 + c_3 x_2 + c_4 x_3 + c_5 x_3^3 + c_6 x_1 + c_7 x_5 + c_8 x_6 + c_9 x_7 + c_{10} x_8 - f(\tau),$$

$$H = d_2 x_2 + d_3 x_1 + d_4 x_1^3 + d_5 x_4 + d_6 x_3 + d_7 x_5 + d_8 x_6 + d_9 x_7 + d_{10} x_8 - g(\tau). \tag{17}$$

Since the aeroelastic equations are formulated as a set of first-order ordinary differential equations, a number of numerical integration methods are available to solve this initial-value problem. The fourth-order Runge–Kutta method is used in the present studies to investigate the effects of initial conditions $\alpha(0)$, $\alpha'(0)$, $\xi(0)$, and $\xi'(0)$ on the flutter boundaries.

In the numerical time integration, Jones & Lee (1985) analysed mechanical systems and pointed out that the accuracy in the amplitude and period of oscillation is affected by the time step $\Delta\tau$. In their study, a value of $\Delta\tau$ equal to 1/256 of the shorter period of the two coupled modes of oscillation was recommended. This value was found to be sufficiently small to give good accuracy while ensuring that the computation time is not excessive. In this study, $\Delta\tau$ is chosen to be 0·1 since the smallest period is approximately 27 for the airfoil parameters used.

2.2. System Stability Near Equilibrium Points

In equation (15) the terms $f(\tau)$ and $g(\tau)$ can be neglected if $\alpha(0) \ll 1$ and $\xi(0) \ll 1$, or $\tau \gg 1$. In this paper, the system behaviour when transients are damped out (that is, $\tau \gg 1$) is studied analytically. The equations governing the airfoil motion are then a set of autonomous differential equations. The equilibrium points of the dynamic system can be obtained by setting right-hand side of equation (15) to zero, that is

$$\mathbf{f}(\mathbf{X}; U^*) = 0. \tag{18}$$

In general, equation (18) has nine solutions with cubic nonlinearities in two degrees of freedom. Only three solutions exist when we consider one cubic nonlinearity in either the pitch or plunge degree of freedom. Simplifying equation (18), we found that there is only one physically meaningful solution denoted as $\mathbf{X}_E$ and is given by

$$\mathbf{X}_E = \{0, 0, 0, 0,\ 0, 0, 0, 0\}^{\mathrm{T}}. \tag{19}$$

Introducing a variable vector $\mathbf{y} = \mathbf{X} - \mathbf{X}_E$, and expanding equation (15) about $\mathbf{X}_E$, we obtain the following equation:

$$\mathbf{y}' = \mathbf{f}(\mathbf{X}_E; U^*) + \left.\frac{\partial \mathbf{f}(\mathbf{X}; U^*)}{\partial \mathbf{X}}\right|_{\mathbf{X}_E} \mathbf{y} + \mathcal{O}(|\mathbf{y}|^2). \tag{20}$$

Equation (20) describes the evolution of the nonlinear system in the vicinity of $\mathbf{X}_E$. Since the system stability near equilibrium points is investigated, the magnitudes of pitch and plunge motion are small and we can neglect higher-order terms. The linearized equation for the nonlinear system can be written as

$$\mathbf{y}' = \mathbf{J}_{\mathbf{X}} \mathbf{y}, \tag{21}$$

where $\mathbf{J}_{\mathbf{X}} = (\partial \mathbf{f}(\mathbf{X}; U^*)/\partial \mathbf{X})|_{\mathbf{X}_E}$, is an 8×8 Jacobian matrix evaluated at $\mathbf{X}_E$ whose terms are written out in full in Lee *et al.* (1998). The solution of equation (21) with initial value $\mathbf{y}(0)$ at $\tau = 0$ is given by

$$\mathbf{y}(\tau) = \mathrm{e}^{\mathbf{J}_{\mathbf{X}}\tau} \mathbf{y}(0). \tag{22}$$

The eigenvalues of $\mathbf{J_X}$ are normally distinct and the complex eigenvalues are of more interest than the real-valued ones. A linear transformation $\mathbf{T}$ can be found (Wiggins 1990) which transforms equation (22) into the following form:

$$\mathbf{y}(\tau) = \mathrm{e}^{\mathbf{T}\Lambda\tau^{-1}}\,\mathbf{y}(0) = \mathbf{T}\mathrm{e}^{\Lambda\tau}\,\mathbf{T}^{-1}\mathbf{y}(0). \tag{23}$$

Here $\mathbf{T}$ is an 8×8 matrix and its columns are the eigenvectors corresponding to the eight eivenvalues of the Jacobian matrix $\mathbf{J_x}$; $\mathbf{T}^{-1}$ is the inverse matrix of $\mathbf{T}$, and Λ is a diagonal matrix with eigenvalues on the main diagonal. In component form equation (23) can be expressed as

$$\mathbf{y}(\tau) = \begin{bmatrix} v_{11} & v_{21} & \cdots & v_{81} \\ v_{12} & v_{22} & \cdots & v_{82} \\ \vdots & \vdots & \cdots & \vdots \\ v_{18} & v_{28} & \cdots & v_{88} \end{bmatrix} \begin{bmatrix} \mathrm{e}^{\lambda_1\tau} & 0 & \cdots & 0 \\ 0 & \mathrm{e}^{\lambda_2\tau} & \cdots & 0 \\ 0 & 0 & \ddots & \vdots \\ 0 & 0 & \cdots & \mathrm{e}^{\lambda_*\tau} \end{bmatrix} \mathbf{T}^{-1}\mathbf{y}(0)$$

$$= \begin{bmatrix} v_{11}\mathrm{e}^{\lambda_1\tau} & v_{21}\mathrm{e}^{\lambda_2\tau} & \cdots & v_{81}\mathrm{e}^{\lambda_*\tau} \\ v_{12}\mathrm{e}^{\lambda_1\tau} & v_{22}\mathrm{e}^{\lambda_2\tau} & \cdots & v_{82}\mathrm{e}^{\lambda_*\tau} \\ \vdots & \vdots & \cdots & \vdots \\ v_{18}\mathrm{e}^{\lambda_1\tau} & v_{28}\mathrm{e}^{\lambda_2\tau} & \cdots & v_{88}\mathrm{e}^{\lambda_*\tau} \end{bmatrix} \begin{Bmatrix} C_1 \\ C_2 \\ \vdots \\ C_8 \end{Bmatrix}, \tag{24}$$

where $v_{i,j}$ is the jth component of the ith eigenvector corresponding to the ith eigenvalue λ_i, and the constant vector $\mathbf{C}$ is defined as

$$\mathbf{C} = \{C_1, C_2, \ldots, C_8\}^{\mathrm{T}} = (\mathbf{T}^{-1}\mathbf{y}(0))^{\mathrm{T}}. \tag{25}$$

In equation (24), the eigenvectors are real or complex conjugates depending whether the eigenvalues are real or complex conjugates. Each real eigenvector is a one-dimensional subspace and each pair of conjugate eigenvectors constructs a two-dimensional subspace. It can be proved (Arnold 1980) that for real initial values of $\mathbf{y}(0)$, the solutions of equation (21) are real-valued. Each two-dimensional subspace composed of conjugate eigenvectors can be transformed into a real two-dimensional subspace if necessary (Wiggins 190).

In a more compact form, equation (24) can be written as

$$y_i(\tau) = \sum_{k=1}^{8} C_k \mathrm{e}^{\lambda_k\tau} v_{ki}, \quad i = 1, \ldots, 8. \tag{26}$$

Equation (26) states that the solution of equation (21) consists of linear combinations of terms invovling components of the exponential operator, the corresponding eigenvectors (both are defined by the eigenvalues) and the initial value vector $\mathbf{y}(0)$. The eigenvalues are functions of the system parameters μ, x_α, r_α, a_h, ζ_α, ζ_ξ, $\bar{\omega}$, Ψ_1, Ψ_2, ε_1, ε_2 and velocity U^*.

If the eigenvalues are not distinct, i.e., if there are multiple eigenvalues, the Jacobian matrix $\mathbf{J_x}$ should be transformed into a standard Jordan block form. Since no multiple eigenvalues are found for a cubic nonlinearity, the expression related to multiple eigenvalues are not required.

2.3. Determination of Hopf Bifurcation Point

Three conditions are required to satisfy the occurrence of Hopf bifurcation (Seydel 1988): (a) the bifurcation occurs at an equilibrium point, i.e., $\mathbf{f}(\mathbf{X}_E; U^*) = 0$; (b) only one pair of conjugate eigenvalues of the Jacobian matrix $\mathbf{J_x}(\mathbf{X}_E; U^*)$ has vanishing real part at this

point; and (c) the derivative of the real part of this pair of conjugate eigenvalues with respect to U^* is not zero at this point, i.e., the "transversality condition" is satisfied,

$$\left.\frac{\mathrm{d}[\mathrm{Re}(\lambda)]}{\mathrm{d}U^*}\right|_{U_E^*} \neq 0. \tag{27}$$

where U_E^* is equal to the nondimensional linear flutter speed U_L^*. A Hopf bifurcation point can be considered as the transition point where a stable equilibrium solution changes to an oscillatory solution with zero amplitude (Seydel 1988). If we consider only periodic oscillation, the terms $f(\tau)$ and $g(\tau)$ can be neglected in equation (15) and we have a system of autonomous equations.

An expanded system to determine the Hopf bifurcation point can be derived by adding a small oscillatory perturbation to an equilibrium point $\mathbf{X}_E$ (Morton & Beran 1996). We assume

$$\mathbf{X} = \mathbf{X}_E + \varepsilon \mathbf{P} \mathrm{e}^{\mathrm{i}\omega\tau} = \varepsilon \mathbf{P} \mathrm{e}^{i\omega\tau}, \tag{28}$$

where ε is a vanishingly small parameter and $\mathbf{P} = \mathbf{P}_1 + \mathrm{i}\mathbf{P}_2$ is a complex eigenvector corresponding to the purely imaginary eigenvalue $\mathrm{i}\omega$. Equation (28) assumes that the system evolution from the perturbation is within the subspace formed by the conjugate eigenvectors corresponding to the conjugate eigenvalue $\pm\mathrm{i}\omega$. Substituting equation (28) into (15) and using Taylor's expansion, we obtain the following equation:

$$\mathrm{i}\varepsilon\omega \mathbf{P} \mathrm{e}^{\mathrm{i}\omega\tau} - \mathbf{f}(\mathbf{X}_E; U^*) - \varepsilon \mathrm{e}^{\mathrm{i}\omega\tau} \mathbf{f}_{\mathbf{X}}(\mathbf{X}_E; U^*)\mathbf{P} + \mathcal{O}(\varepsilon^2) = \mathbf{0}. \tag{29}$$

Since $\mathbf{f}(\mathbf{X}_E; U^*) = 0$, neglecting higher-order terms we obtain

$$\mathrm{i}\omega \mathbf{P} - \mathbf{f}_{\mathbf{X}}(\mathbf{X}_E; U^*)\mathbf{P} = \mathbf{0}, \tag{30}$$

which can be written as

$$\begin{aligned} \omega \mathbf{P}_2 + \mathbf{f}_{\mathbf{X}}(\mathbf{X}_E; U^*)\mathbf{P}_1 &= \mathbf{0}, \\ -\omega \mathbf{P}_1 + \mathbf{f}_{\mathbf{X}}(\mathbf{X}_E; U^*)\mathbf{P}_2 &= \mathbf{0}. \end{aligned} \tag{31}$$

To uniquely define the eigenvector $\mathbf{P}$, vectors $\mathbf{P}_1$ and $\mathbf{P}_2$ are normalized by the following constraints:

$$\mathbf{q}^{\mathrm{T}}\mathbf{P}_1 = 0, \quad \mathbf{q}^{\mathrm{T}}\mathbf{P}_2 = 1, \tag{32}$$

where $\mathbf{q}$ is a normalization vector. The components of $\mathbf{P}_1$ and $\mathbf{P}_2$ are initialized by assigning an arbitrary value to them, and following Morton & Beran (1996), $\boldsymbol{q}$ is formed by the relationship

$$\mathbf{q} = \frac{\mathbf{P}_2}{\mathbf{P}_2^{\mathrm{T}}\mathbf{P}_2}, \tag{33}$$

which satisfies the second normalization condition in equations (32). Combining equations (31) and (32) we obtain an expanded system to determine the Hopf bifurcation point given by the following equations:

$$\mathbf{F}(\mathbf{Y}) = \begin{bmatrix} \mathbf{f}_{\mathbf{X}}(\mathbf{X}_E; U^*)\mathbf{P}_1 + \omega \mathbf{P}_2 \\ \mathbf{q}^{\mathrm{T}}\mathbf{P}_1 \\ \mathbf{f}_{\mathbf{X}}(\mathbf{X}_E; U^*)\mathbf{P}_2 - \omega \mathbf{P}_1 \\ \mathbf{q}^{\mathrm{T}}\mathbf{P}_2 - 1 \end{bmatrix} = \mathbf{0}, \quad \mathbf{Y} = \begin{Bmatrix} \mathbf{P}_1 \\ U^* \\ \mathbf{P}_2 \\ \omega \end{Bmatrix}, \tag{34}$$

where $\mathbf{Y}$ is the variable vector with 18 components; $\mathbf{F}(\mathbf{Y})$ represents the function vector of the 18 functions and the individual terms are given in Lee *et al.* (1998).

Using Newton's iteration method the above equation can be written as

$$\mathbf{F}_{\mathbf{Y}}(\mathbf{Y})\Delta\mathbf{Y} = -\mathbf{F}(\mathbf{Y}), \tag{35}$$

where $\mathbf{F}_{\mathbf{Y}}(\mathbf{Y})$ is the Jacobian matrix of $\mathbf{F}(\mathbf{Y})$, and $\Delta\mathbf{Y}$ is the increment of $\mathbf{Y}$ used in the next iteration. The Jacobian matrix $\mathbf{F}_{\mathbf{Y}}(\mathbf{Y})$ in block-matrix form is given by

$$\mathbf{F}_{\mathbf{Y}}(\mathbf{Y}) = \begin{bmatrix} \mathbf{f}_{\mathbf{X}}(\mathbf{X}_E; U^*) & \{\mathbf{f}_{\mathbf{X}}(\mathbf{X}_E; U^*)\mathbf{P}_1\}_{U^*} & \omega\mathbf{I} & \mathbf{P}_2 \\ \mathbf{q}^{\mathrm{T}} & 0 & 0 & 0 \\ -\omega\mathbf{I} & \{\mathbf{f}_{\mathbf{X}}(\mathbf{X}_E; U^*)\mathbf{P}_2\}_{U^*} & \mathbf{f}_{\mathbf{X}}(\mathbf{X}_E; U^*) & -\mathbf{P}_1 \\ 0 & 0 & \mathbf{q}^{\mathrm{T}} & 0 \end{bmatrix}, \tag{36}$$

where $\mathbf{I}$ is the identity matrix. The elements of the Jacobian matrix $\mathbf{F}_{\mathbf{Y}}(\mathbf{Y})$ are also given in Lee *et al.* (1998). In equation (36), $\mathbf{f}_{\mathbf{X}}(\mathbf{X}_E; U^*)$ is an 8×8 Jacobian matrix evaluated at $\mathbf{X} = \mathbf{X}_E$, and $\{\mathbf{f}_{\mathbf{X}}(\mathbf{X}_E; U^*)\mathbf{P}_i\}_{U^*}$ is an eight-component vector of the derivative of the product of $\mathbf{f}_{\mathbf{X}}(\mathbf{X}_E; U^*)$ and $\mathbf{P}_i$ $(i = 1, 2)$ with respect to U^*.

2.4. Amplitudes of Pitch and Plunge Motion of Limit Cycle Oscillation

An airfoil with a cubic structural nonlinearity is unstable at equilibrium points $U^* > U_l^*$. For $\beta_\alpha > 0$, a small perturbation will grow initially and reach a limit cycle state after a transient period. In the analysis given by Lee *et al.* (1997) for large time τ, the transient terms $f(\tau)$ and $g(\tau)$ in equations (10) and (11) damp out and we have a system of autonomous equations. We assume the plunge and pitch motions to be of the following form:

$$\begin{aligned} \xi(\tau) &= a_1(\tau)\cos(\omega\tau) + b_1(\tau)\sin(\omega\tau), \\ \alpha(\tau) &= a_2(\tau)\cos(\omega\tau) + b_2(\tau)\sin(\omega\tau), \end{aligned} \tag{37}$$

and w_i $(i = 1, 2, 3, 4)$ can be written as follows:

$$\begin{aligned} w_1(\tau) &= a_3(\tau)\cos(\omega\tau) + b_3(\tau)\sin(\omega\tau), \\ w_2(\tau) &= a_4(\tau)\cos(\omega\tau) + b_4(\tau)\sin(\omega\tau), \\ w_3(\tau) &= a_5(\tau)\cos(\omega\tau) + b_5(\tau)\sin(\omega\tau), \\ w_4(\tau) &= a_6(\tau)\cos(\omega\tau) + b_6(\tau)\sin(\omega\tau), \end{aligned} \tag{38}$$

where a_i and b_i $(i = 1, \ldots, 6)$ are assumed to be slowly varying functions of τ, and ω is the angular frequency of the LCO. The second time derivatives are considered to be small thus neglected. This approach is often used in perturbation analysis (Jordan & Smith 1983).

Note that $\xi^3(\tau)$ and $\alpha^3(\tau)$ can be written as

$$\begin{aligned} \xi^3(\tau) &= \tfrac{3}{4}r^2[a_1(\tau)\cos(\omega\tau) + b_1(\tau)\sin(\omega\tau)] + \{\text{higher harmonics in } 3\omega\tau\}, \\ \alpha^3(\tau) &= \tfrac{3}{4}R^2[a_2(\tau)\cos(\omega\tau) + b_2(\tau)\sin(\omega\tau)] + \{\text{higher harmonics in } 3\omega\tau\}, \end{aligned} \tag{39}$$

where $r^2 = a_1^2 + b_1^2$, $R^2 = a_2^2 + b_2^2$ and r and R denote the amplitude of ξ and α, respectively. Assuming the higher harmonic terms in equations (39) to be small and substituting equations (37), (38) and (39) into (9), (10) and (11), we obtain a system of 12 first-order

nonlinear ordinary differential equations after matching the coefficients of $\cos(\omega\tau)$ and $\sin(\omega\tau)$. The resulting equations in matrix form are

$$\mathbf{M}\mathbf{Z}' = \mathbf{Q}(\mathbf{Z}), \tag{40}$$

where the matrix $\mathbf{M}$ in block form is

$$\mathbf{M} = \begin{bmatrix} \mathbf{H} & \mathbf{0} \\ \mathbf{0} & \mathbf{I} \end{bmatrix}, \tag{41}$$

with

$$\mathbf{H} = \begin{bmatrix} c_2 & 2\omega c_0 & c_3 & 2\omega c_1 \\ -2\omega c_0 & c_2 & -2\omega c_1 & c_3 \\ d_5 & 2\omega d_0 & d_2 & 2\omega d_1 \\ -2\omega d_0 & d_5 & -2\omega \mathrm{d}_1 & d_2 \end{bmatrix}, \tag{42}$$

and $\mathbf{I}$ is an 8×8 identity matrix.

In equation (40), $\mathbf{Z}$ is a variable vector given by

$$\mathbf{Z} = \{a_1, b_1, a_2, \ldots, a_6, b_6\}^{\mathrm{T}}, \tag{43}$$

and $\mathbf{Q}(\mathbf{Z})$ is the function vector

$$\mathbf{Q}(\mathbf{Z}) = [Q_1(\mathbf{Z}), Q_2(\mathbf{Z}), \ldots, Q_{12}(\mathbf{Z})]^{\mathrm{T}}, \tag{44}$$

whose terms are defined in Lee *et al.* (1998). Since the amplitudes of LCO do not change with time, we can set $a_i' = 0$ and $b_i' = 0$ and obtain a system of 12 algebraic equations. In deriving the expressions for a_1, b_1, a_2, and b_2, equation (40) is first solved for $a_3, b_3, \ldots, a_6$ and b_6 which are then substituted into the expressions for a_1, b_1, a_2, and b_2 to give a set of nonlinear algebraic equations. Following Lee *et al.* (1997), a quadratic equation for R^2 can be written as follows:

$$R^4 + \frac{2s_2}{q_2} R^2 + C = 0. \tag{45}$$

where

$$C = \frac{1}{q_2^2}\{n_2^2 + s_2^2 - (p_2^2 + m_2^2)A\}, \tag{46}$$

and

$$A = \frac{(n_1^2 + s_1^2)}{[m_1^2 + (p_1 + q_1 r^2)^2]}. \tag{47}$$

The coefficients $m_1, n_1, \ldots$ are given in Lee *et al.* (1998). Note that these coefficients are functions of the systems parameters, velocity, U^*, and the angular frequency ω of LCO.

The plunge amplitude is given by

$$r^2 = AR^2. \tag{48}$$

In this study, we consider only a cubic nonlinearity in the pitch DOF. Setting $\beta_\xi = c_5 = q_1 = 0$, equation (47) becomes

$$A = \frac{(n_1^2 + s_1^2)}{(m_1^2 + p_1^2)}. \tag{49}$$

Finally, we can get the following simple expression of the amplitude of pitch motion of LCO:

$$R^2 = \frac{1}{q_2}\{-s_2 \pm \sqrt{(p_2^2 + m_2^2)A - n_2^2}\}, \tag{50}$$

and the amplitude of plunge motion is given by equation (48).

3. RESULTS AND DISCUSSION

In Lee & LeBlanc's (1986) studies, only a cubic structural nonlinearity in the pitch degree of freedom was considered, and β_ξ in equation (1) was set to zero. In this paper, we use equation (15) to recompute a number of cases from Lee & LeBlanc's (1986) report and demonstrate that the two methods give identical results. The elastic axis of the airfoil is placed at the $\frac{1}{4}$ chord point (that is $a_h = -\frac{1}{2}$), $\zeta_\xi = \zeta_\alpha = 0$ and r_α is kept constant at 0·5. Other properties of the airfoil, such as μ, x_α $\bar{\omega}$ and β_α are varied.

The deviation from linearity of the restoring moment is shown in Figure 2 where the term $\alpha + \beta_\alpha \alpha^3$ in equation (2) is plotted against α for three values of β_α up to ± 3. At the maximum value of $\beta_\alpha = 3$, the contribution of the cubic term is about 37% at $\alpha = 20^\circ$,

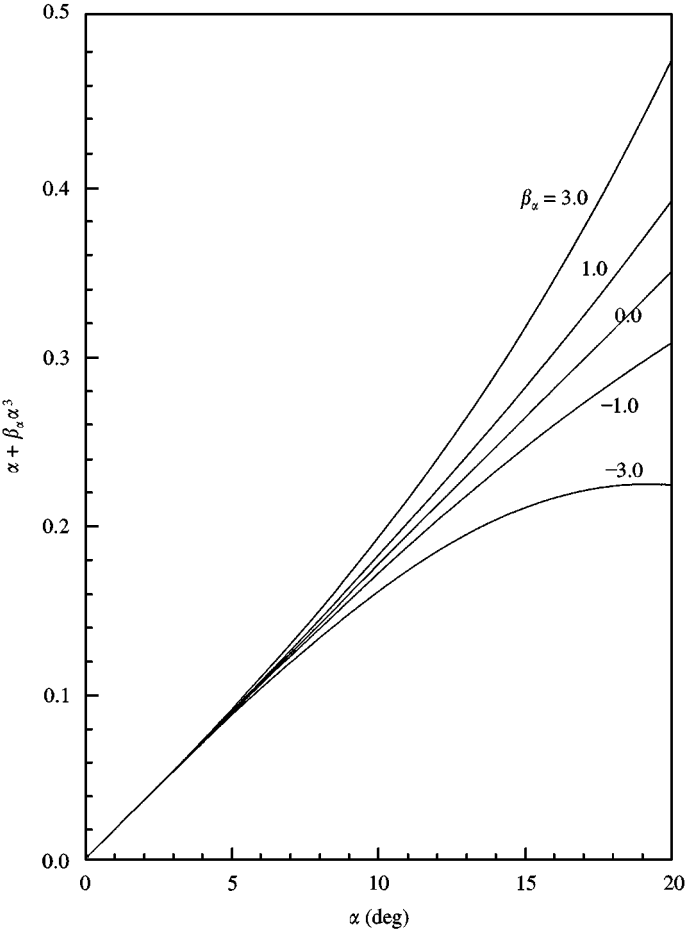

Figure 2. Effects of β_α on nonlinear moment.

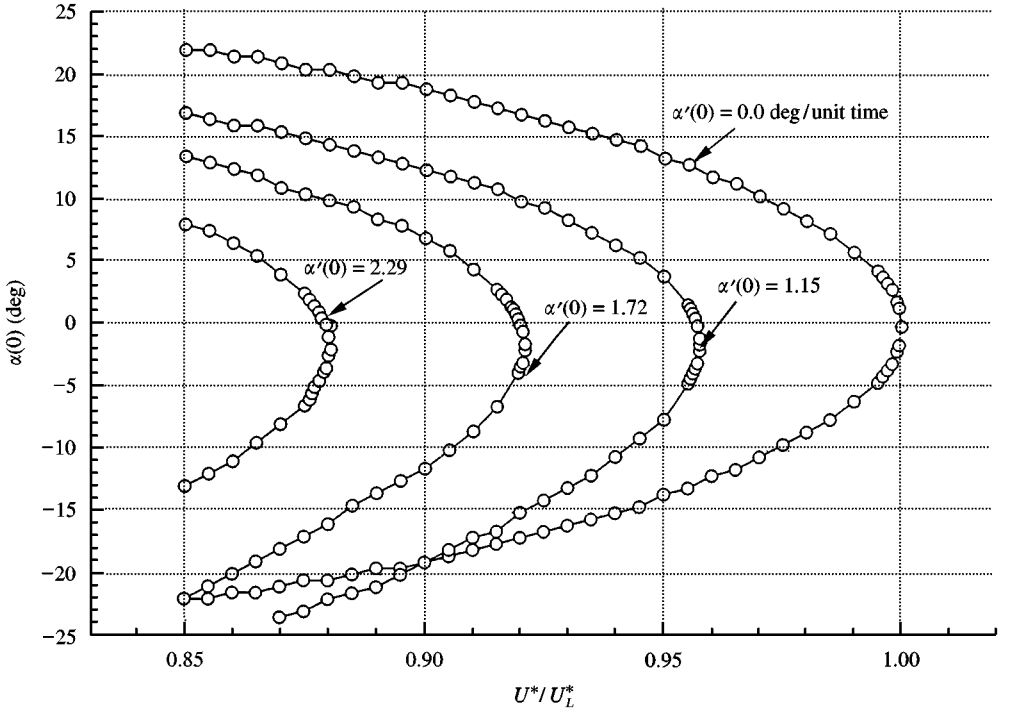

Figure 3. Flutter boundary ($\alpha(0)$ versus U^*/U_L^*) for soft spring: $\bar{\omega} = 0{\cdot}2$, $\mu = 100$, $a_h = -0.5$, $x_\alpha = 0{\cdot}25$, $r_\alpha = 0{\cdot}5$, $\zeta_\alpha = \zeta_\xi = 0$ and $\beta_\alpha = -3$.

approximately 20% at $\alpha = 15^\circ$, and can be neglected for $\alpha < 5^\circ$. For values of α where the aerodynamics given by equations (6) and (7) is applicable (α approximately under 15°), the nonlinear term can be considered small and the system is dominated by the linear stiffness.

3.1. Flutter Boundaries for Soft Spring

For a soft spring, β_α is negative, and we investigate the effects of initial conditions by a numerical simulation study. The linear flutter velocity U_L^* is used as a reference velocity and is determined numerically by setting the nonlinear term β_α to be zero. By observing the converging and diverging behaviour of the time series, we can determine the linear flutter velocity for the selected system parameters.

Figure 3 shows flutter boundaries for $-22^\circ < \alpha(0) <$ to 22° and $\alpha'(0) = 0{\cdot}0$, $1{\cdot}15$, $1{\cdot}72$ and $2{\cdot}29^\circ$ unit time while kept $\xi(0) = \xi'(0) = 0$. The motion is unstable to the right of the flutter boundary. The airfoil parameters are : $\mu = 100$, $\bar{\omega} = 0{\cdot}2$, $r_\alpha = 0{\cdot}5$, $a_h = -1/2$, $x_\alpha = 0{\cdot}25$ and $\beta_\alpha = -3{\cdot}0$. The ranges of $\alpha(0)$ and $\alpha'(0)$ are selected so that the linear aerodynamics given in equations (6) and (7) can be used, except for $\alpha(0)$ greater than approximately 15° where the limitations of the aerodynamic terms are probably reached. The destabilizing effect of a soft spring is illustrated in this figure which shows that flutter can be induced at a velocity U^* below the linear flutter velocity U_L^*. This effect increases with increasing $\alpha'(0)$. The flutter boundary curve for $\alpha'(0) = 0$ is symmetrical about the axis $\alpha(0) = 0$. For the other three values of $\alpha'(0)$, the flutter boundaries are not symmetrical, because a positive velocity is given to the airfoil initially.

Figure 4 shows the destabilizing effect of initial $\alpha'(0)$ on the flutter boundaries for $-3 < \alpha'(0) < 3^\circ$/unit time at $\alpha(0) = 0^\circ, 5^\circ, 10^\circ, 15^\circ$ for the same values of μ, β_α, x_α, r_α and $\bar{\omega}$.

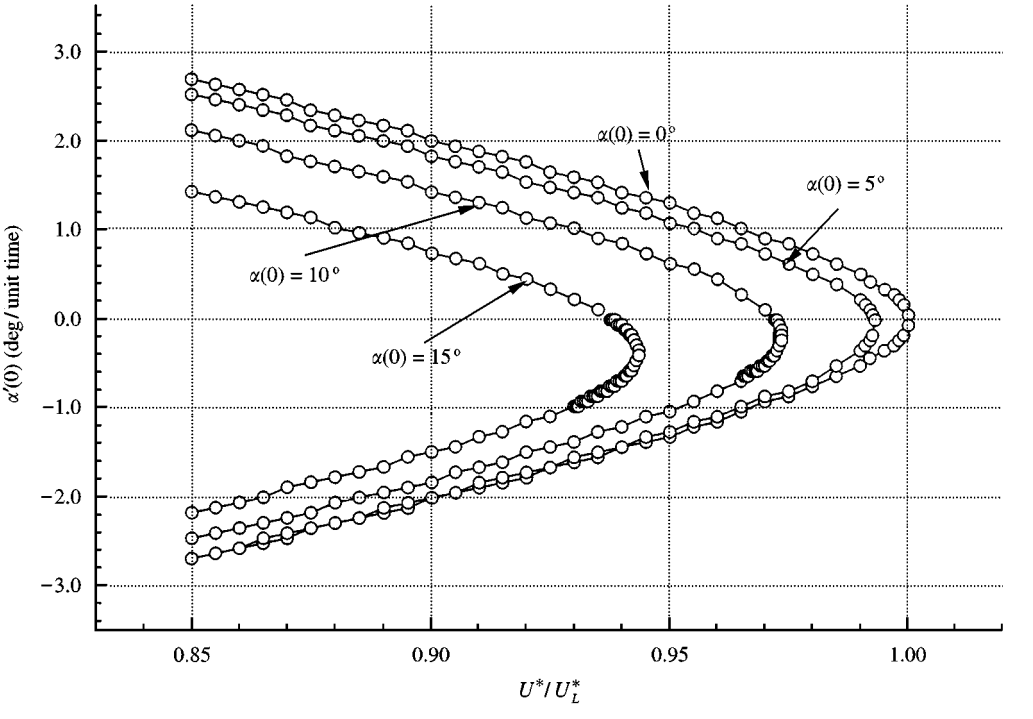

Figure 4. Flutter boundary ($\alpha'(0)$ versus U^*/U_L^*) for soft spring: $\bar{\omega} = 0{\cdot}2$, $\mu = 100$, $a_h = -0.5$, $x_\alpha = 0{\cdot}25$, $r_\alpha = 0{\cdot}5$, $\zeta_\alpha = \zeta_\xi = 0$ and $\beta_\alpha = -3$.

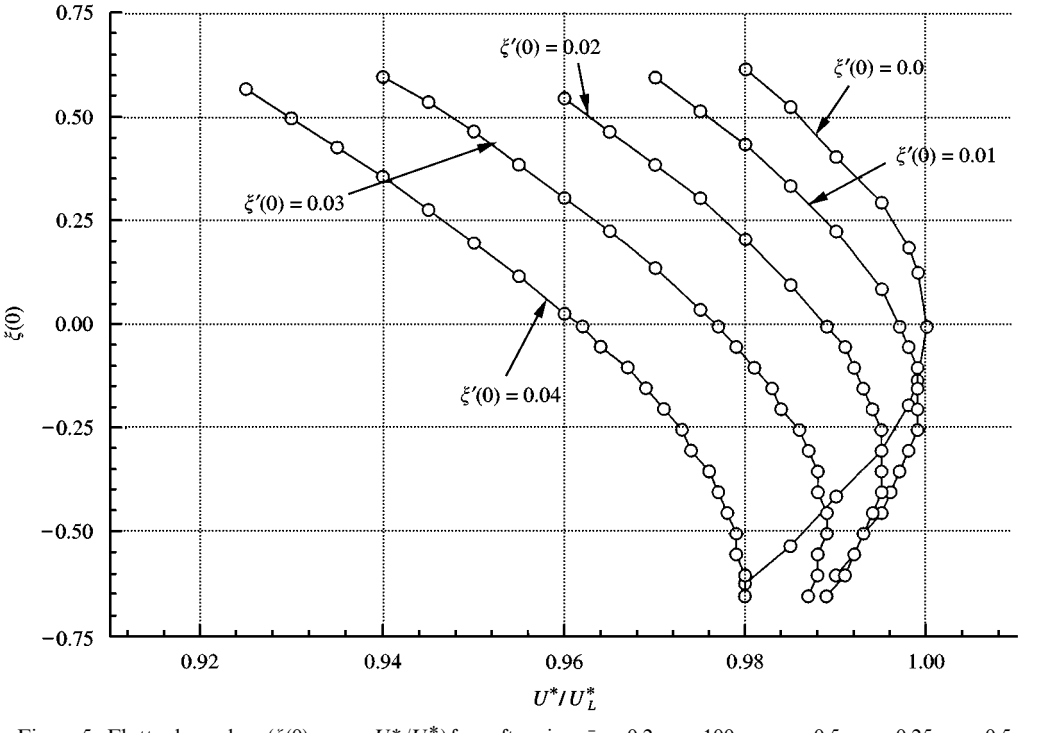

Figure 5. Flutter boundary ($\xi(0)$ versus U^*/U_L^*) for soft spring: $\bar{\omega} = 0{\cdot}2$, $\mu = 100$, $a_h = -0.5$, $x_\alpha = 0{\cdot}25$, $r_\alpha = 0{\cdot}5$, $\zeta_\alpha = \zeta_\xi = 0$ and $\beta_\alpha = -3$.

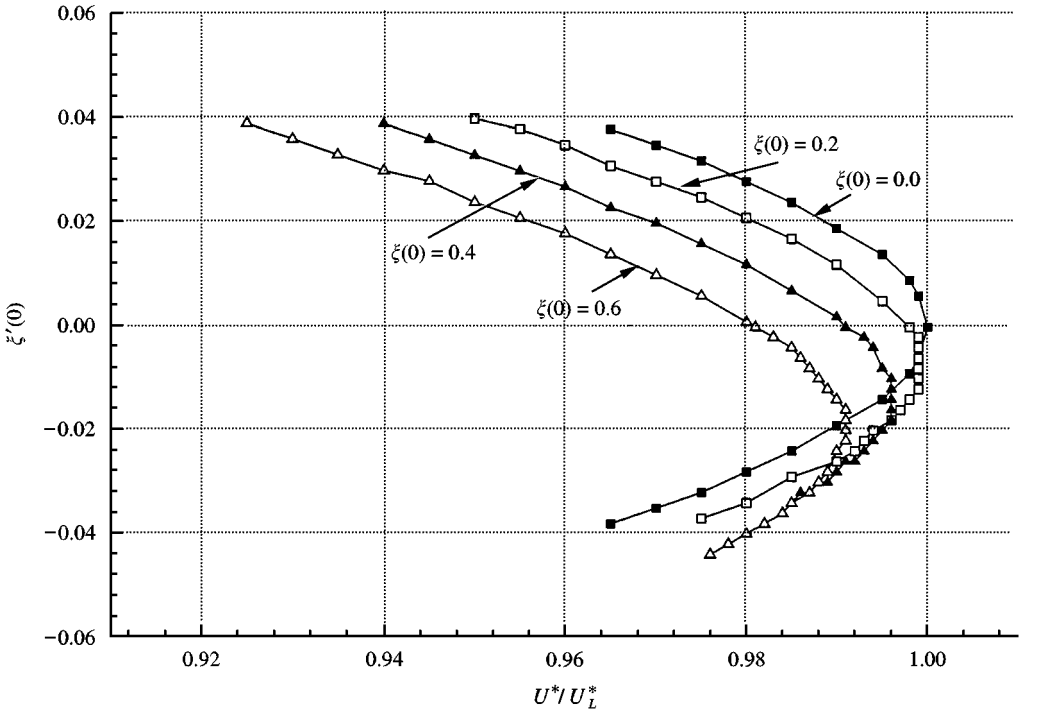

Figure 6. Flutter boundary ($\xi'(0)$ versus U^*/U_L^*) for soft spring: $\bar{\omega} = 0{\cdot}2$, $\mu = 100$, $a_h = -0.5$, $x_\alpha = 0{\cdot}25$, $r_\alpha = 0{\cdot}5$, $\zeta_\alpha = \zeta_\xi = 0$ and $\beta_\alpha = -3$.

As expected, the curve for $\alpha(0) = 0^\circ$ is symmetric about the axis $\alpha'(0) = 0$, while for $\alpha(0) > 0$ the flutter boundaries are displaced downwards and the amount of the shift increases with $\alpha(0)$.

The flutter boundaries for $-0{\cdot}6 < \xi(0) < 0{\cdot}6$ corresponding to $\xi'(0) = 0{\cdot}0, 0{\cdot}01, 0{\cdot}02, 0{\cdot}03$ and $0{\cdot}04$ are shown in Figure 5 for the same values of μ, β_α, x_α, r_α and $\bar{\omega}$. The criterion for selecting the ranges of $\xi(0)$ and $\xi'(0)$ is similar to that for $\alpha(0)$ and $\alpha'(0)$, that is, the amplitudes of plunge and pitch motions are sufficiently small for the linear aerodynamics to be applicable. The flutter boundary for $\xi'(0) = 0$ is symmetric with respect to the $\xi(0)$ axis, while for other values of $\xi'(0)$ it is highly nonsymmetric. The value of $\xi(0)$ at the maximum U^*/U_L^* moves downwards in the negative $\xi(0)$ direction. Each of the curves for which $\xi'(0) \neq 0$ intersects with the flutter boundary for $\xi'(0) = 0$ in the region of negative $\xi(0)$.

Figure 6 gives the flutter boundaries for $-0{\cdot}04 < \xi'(0) < 0{\cdot}04$ at $\xi(0) = 0{\cdot}0, 0{\cdot}2, 0{\cdot}4, 0{\cdot}6$ for the same values of μ, β_α, x_α, r_α and $\bar{\omega}$. The curves cross each other in the region of negative $\xi'(0)$.

The flutter boundary is affected by the system parameters, such as μ, β_α, $\bar{\omega}$ and x_α. These effects have been studied by Lee LeBlanc (1986), who showed that increasing μ has a destabilizing effect and the boundary curves are all displaced more towards the left for the larger values of μ. The effect is more pronounced as the value of β_α decreases.

Increasing the distance between the centre of mass and the elastic axis has a stabilizing effect, and results from Lee & LeBlanc (1986) at $\mu = 250$ show the flutter boundaries to move closer to the linear flutter speed as x_α is increased. In the same report, the effect of $\bar{\omega}$ was investigated, and the results show that, as the uncoupled natural frequency for plunging motion approaches that of the pitching motion, the flutter boundaries move closer

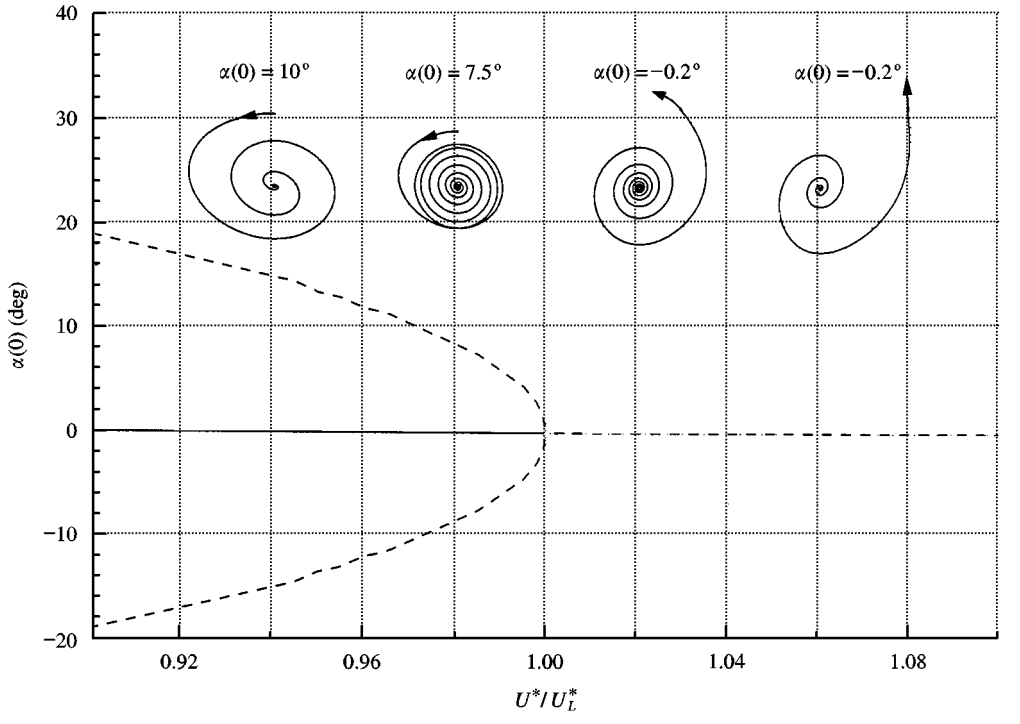

Figure 7. Subcritical Hopf bifurcation for a soft spring with $\beta_\alpha = -3$.

to the linear flutter boundary and the destabilizing effect becomes smaller. At $\bar{\omega} = 1{\cdot}2$, it was shown (Lee & LeBlanc 1986) that the flutter boundaries are virtually independent on the coefficient β_α.

The system stability near equilibrium points can be presented in a plot similar to a bifurcation diagram. For $\beta_\alpha < 0$, a subcritical Hopf bifurcation (Thompson & Stewart 1986) occurs at $U^*/U_L^* = 1$. In Figure 7, $\alpha(0)$ is plotted against U^*/U_L^* for $\alpha(0)' = \xi(0) = \xi'(0) = 0$ with $\beta_\alpha = -3{\cdot}0$, $\mu = 100$, $\bar{\omega} = 0{\cdot}2$, $x_\alpha = 0{\cdot}25$ and $r_\alpha = 0{\cdot}5$. The dotted lines for $U^*/U_L^* \leq 1{\cdot}0$ is the flutter boundary. For values of $\alpha(0)$ bounded by these two curves, the motion is stable. The inset of four figures showing the trajectories of the pitch oscillation are plotted in the phase plane (α' versus α). They are obtained at $U^*/U_L^* = 0{\cdot}94, 0{\cdot}98, 1{\cdot}02, 1{\cdot}06$ and $\alpha(0) = 10, 7{\cdot}5, -0{\cdot}2$ and $-0{\cdot}2^\circ$, respectively. The system converges to the equilibrium points ($\alpha' = \alpha = 0$) for $U^*/U_L^* < 1{\cdot}0$ and diverges away from the unstable equilibrium points ($\alpha' = \alpha = 0$) for $U^*/U_L^* > 1{\cdot}0$. The Hopf bifurcation point is located at $U^*/U_L^* = 1$.

3.2. Flutter Boundaries for Hard Spring

For positive values of β_α (hard spring), divergent flutter is not encountered. Instead, the flutter boundaries [e.g. $\alpha(0)$ versus U^*/U_L^*] for all β_α coalesce into a straight line at the linear flutter speed. This was shown by Woolston *et al.* (1955, 1957) and numerically by Lee & LeBlanc (1986) for a cubic nonlinearity in the pitch degree of freedom and various airfoil parameters. To the right of this boundary, the oscillations maintain a self-limited amplitude which is independent of the initial angular displacement $\alpha(0)$.

For a given $\alpha(0)$, the time it takes for the airfoil motion to reach a steady value depends on the velocity ratio U^*/U_L^*. If a solution is required very close to the flutter boundary, a large

number of cycles of oscillations have to be computed. Using the same airfoil parameters as those for a soft spring described in the last section, (that is, $\mu = 100$, $\bar{\omega} = 0{\cdot}2$, $x_\alpha = 0{\cdot}25$, $r_\alpha = 0{\cdot}5$), Lee & LeBlanc (1986) showed that at $\beta_\alpha = 0{\cdot}3$ it takes approximately 250 cycles for the solution to decay to practically zero values at $U^*/U_L^* = 0{\cdot}9992$ (0·08% less than linear flutter speed) with initial amplitude $\alpha(0) = 10^\circ$ and $\alpha(0)' = \xi(0) = \xi'(0) = 0$. At smaller values of $\alpha(0) = 1^\circ$ and 3°, it requires approximately the same number of cycles for the oscillation amplitude to reach zero value. In the LCO region where $U^*/U_L^* > 1$, the time it takes to reach steady values depends on initial conditions. At $U^*/U_L^* = 1{\cdot}0008$ (0·08% greater than linear flutter speed), the solution takes 130 cycles at $\alpha(0) = 10^\circ$ to reach constant amplitude compared to 190 cycles at $\alpha(0) = 1^\circ$. Increasing the value of U^*/U_L^* increases the convergence rate. At $U^*/U_L^* = 1{\cdot}0024$, steady pitch amplitudes are reached after 60 and 100 cycles for $\alpha(0) = 10^\circ$ and 1°, respectively. Equation (15) has been used to repeat Lee & LeBlanc's (1986) investigation and identical results were obtained. It was found that when large values of β_α were used, the time it takes to decay to a zero value ($U^*/U_L^* < 1$) or reach a constant value ($U^*/U_L^* > 1$) is considerably shorter than those at $\beta_\alpha = 0{\cdot}3$ shown in Lee & LeBlanc's (1986) report.

Lee & LeBlanc (1986) concluded from a number of case studies for different airfoil parameters that there is no noticeable change in the amplitude of the pitch motion when the airfoil/air-mass ratio is varied, while the plunge amplitude increases with an increase in that ratio. Increasing the distance between the centre of mass and the elastic axis results in a larger pitch amplitude while the plunge amplitude gets smaller. As the ratio of the uncoupled natural frequencies of the plunge to pitch motion approaches and exceeds unity, there is an increase in the pitch amplitude while a much larger drop in the plunge amplitude is detected.

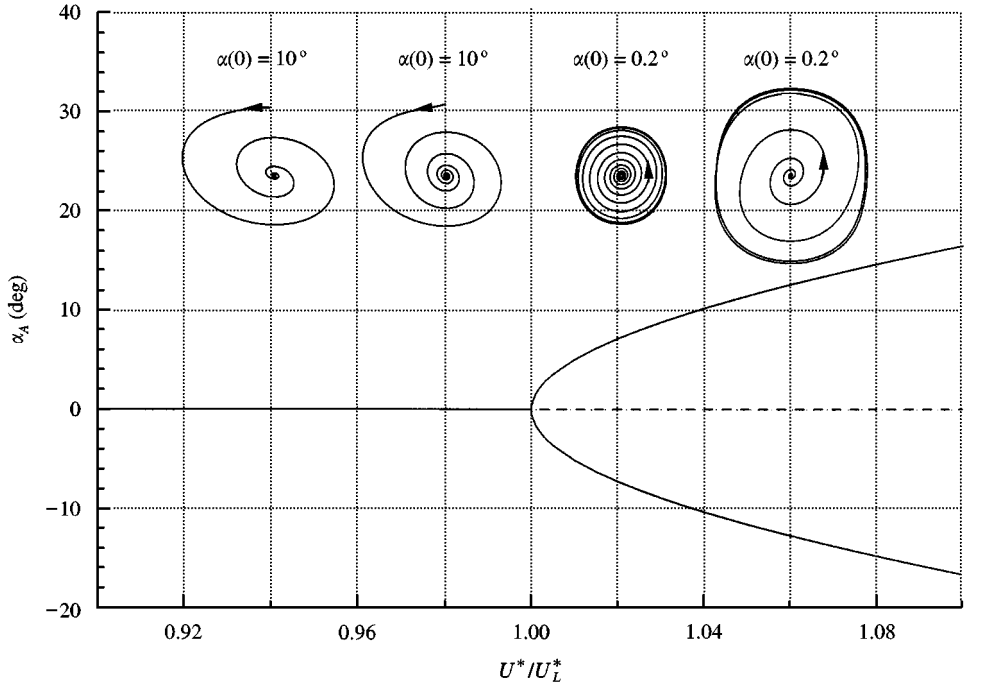

Figure 8. Supercritical Hopf bifurcation for a hard spring with $\beta_\alpha = 3$.

Similarly to Figure 7 the stability behaviour of the airfoil near equilibrium points can be presented in a bifurcation diagram. For $\beta_\alpha = 3$, $\mu = 100$, $\bar{\omega} = 0{\cdot}2$, $a_h = -1/2$ and $x_\alpha = 0{\cdot}25$, Figure 8 shows a plot of the pitch amplitude α_A against U^*/U_L^*. This figure is obtained by varying $\alpha(0)$ only, while keeping $\alpha'(0) = \xi(0) = \xi'(0) = 0$. For $U^*/U_L^* < 1$, the solution is stable for all initial displacement $\alpha(0)$. The solutions in the phase plane (α' versus α) at $U^*/U_L^* = 0{\cdot}94$, $\alpha(0) = 10^\circ$ and $U^*/U_L^* = 0{\cdot}98$, $\alpha(0) = 10^\circ$ are shown in the inset. The phase curve spirals into the origin ($\alpha' = \alpha = 0$) for all $\alpha(0)$, showing the solution to be stable for $U^*/U_L^* < 1$. For $U^*/U_L^* > 1$, the two insets of the phase diagram at $U^*/U_L^* = 1{\cdot}02$ and $1{\cdot}04$ for $\alpha(0) = 0{\cdot}2^\circ$ show the trajectories to spiral away from the origin and becomes periodic with constant amplitude. The solid line shows the amplitude of pitch motion α_A obtained numerically using equation (15). This value is independent of initial displacement $\alpha(0)$ since all solutions with different $\alpha(0)$ will eventually reach a limit-cycle state. The transition from a stable equilibrium solution to limit cycle oscillation is known as a supercritical Hopf bifurcation (Thompson & Stewart 1986).

3.3. System Behaviour Near Equilibrium Points

For various values of U^*/U_L^* with $\mu = 100$, $x_\alpha = 0{\cdot}25$, $r_\alpha = 0{\cdot}5$ and $\bar{\omega} = 0{\cdot}2$, the eigenvalues of the Jacobian matrix at equilibrium points can be calculated using equation (21). The elements of $\mathbf{J_X}$ are given in Lee *et al.* (1998) and β_α appears only in the term d_4 [see Lee *et al.* (1997)]. Since the eigenvalues are evaluated at the equilibrium points where $x_1 = x_2 = \cdots x_8 = 0$, the term containing d_4 becomes zero and the eigenvalues are independent of β_α. The solution of the Jacobian matrix for a given value of U^*/U_L^* has eight eigenvalues. There are two pairs of conjugate eigenvalues (denoted by models I and II) and their real and

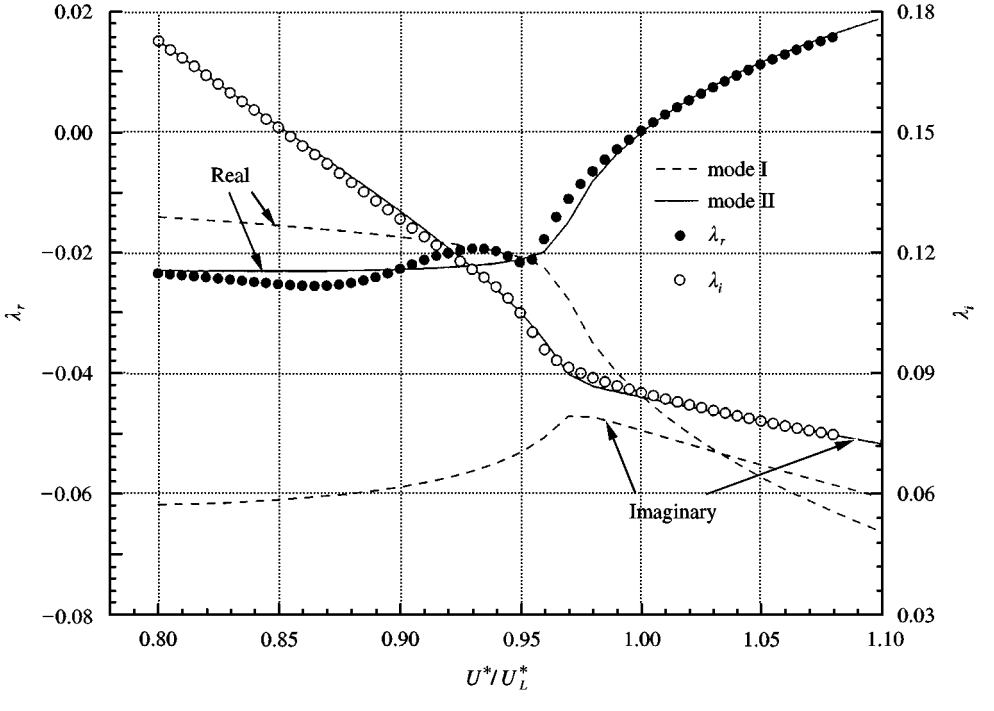

Figure 9. Variation of λ with U^*/U_L^* for the pitch motion with $\bar{\omega} = 0{\cdot}2$, $\mu = 100$, $a_h = -0{\cdot}5$, $x_\alpha = 0{\cdot}25$, $r_\alpha = 0{\cdot}5$, $\zeta_\alpha = \zeta_\xi = 0$ and $\beta_\alpha = 3$.

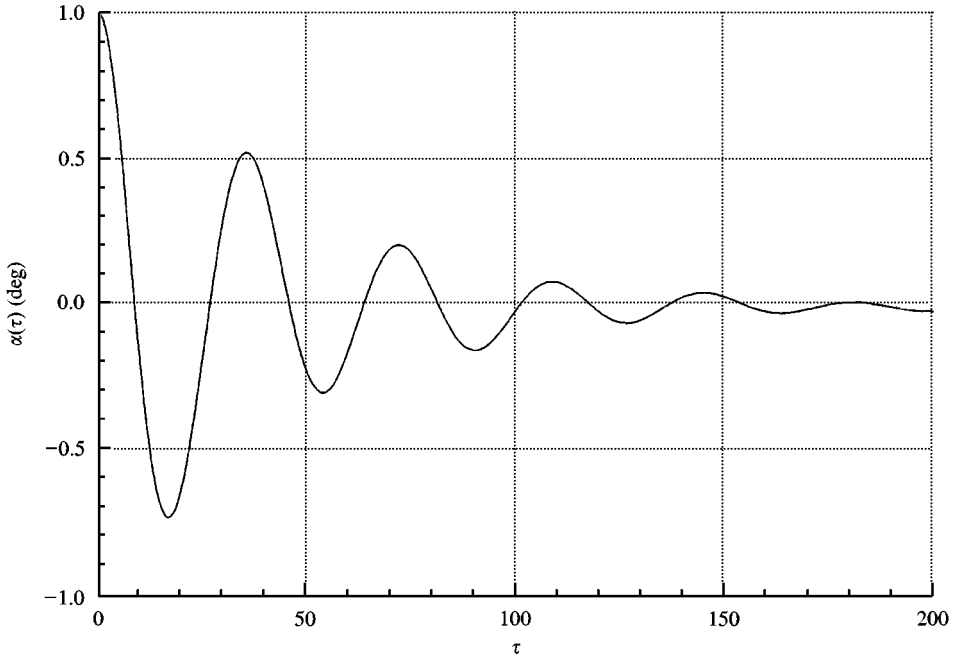

Figure 10. Time series of pitch motion at $U^*/U_L^* = 0{\cdot}8$ with $\bar{\omega} = 0{\cdot}2$, $\mu = 100$, $a_h = -0.5$, $x_\alpha = 0{\cdot}25$, $r_\alpha = 0{\cdot}5$, $\zeta_\alpha = \zeta_\xi = 0$ and $\beta_\alpha = 3$.

imaginary parts are plotted against U^*/U_L^* in Figure 9 (denoted by dashed and solid lines respectively). The other four eigenvalues have zero imaginary parts and they do not represent oscillatory motion.

On examining a typical time series of α from numerical integration of equation (15) (Figure 10), we see that the pitch motion can be adequately represented by a single mode. We can denote the pitch motion by $\alpha = \alpha_0 \exp[(\lambda_r + \mathrm{i}\lambda_i)]\tau$, where α_0 is a constant, λ_r and λ_i are the real and imaginary part of the exponential coefficient λ. Superimposed in Figure 9 are results obtained from numerical simulation for $\beta_\alpha = 3$. The initial conditions are $\alpha(0) = 1^\circ$ (for $U^*/U_L^* < 1$) and $\alpha(0) = 0{\cdot}1^\circ$ (for $U^*/U_L^* > 1$) with $\alpha'(0) = \xi(0) = \xi'(0) = 0$. The imaginary part λ_i is calculated by the following equation:

$$\lambda_i = \frac{2\pi(n_2 - n_1)}{\tau_2 - \tau_1}, \tag{51}$$

where times τ_2 and τ_1 correspond to cycle numbers n_2 and n_1, respectively. The real part λ_r is determined by

$$\lambda_r = \frac{\log \alpha_{2A} - \log \alpha_{1A}}{\tau_2 - \tau_1}, \tag{52}$$

where α_{1A} and α_{2A} are the amplitudes of pitch angles corresponding to τ_2 and τ_1.

The maximum values of α_{1A} and α_{2A} are kept below 10° in the numerical simulation. The first $\frac{1}{2}$ to $3\frac{1}{2}$ cycles in the time series are used to calculate λ_r and λ_i.

The analytical and numerical simulation results are in excellent agreement for mode II for $U^*/U_L^* > 1$. However, for $U^*/U_L^* < 1$, the results from numerical simulation have some scatter about the analytical solution in λ_r only.

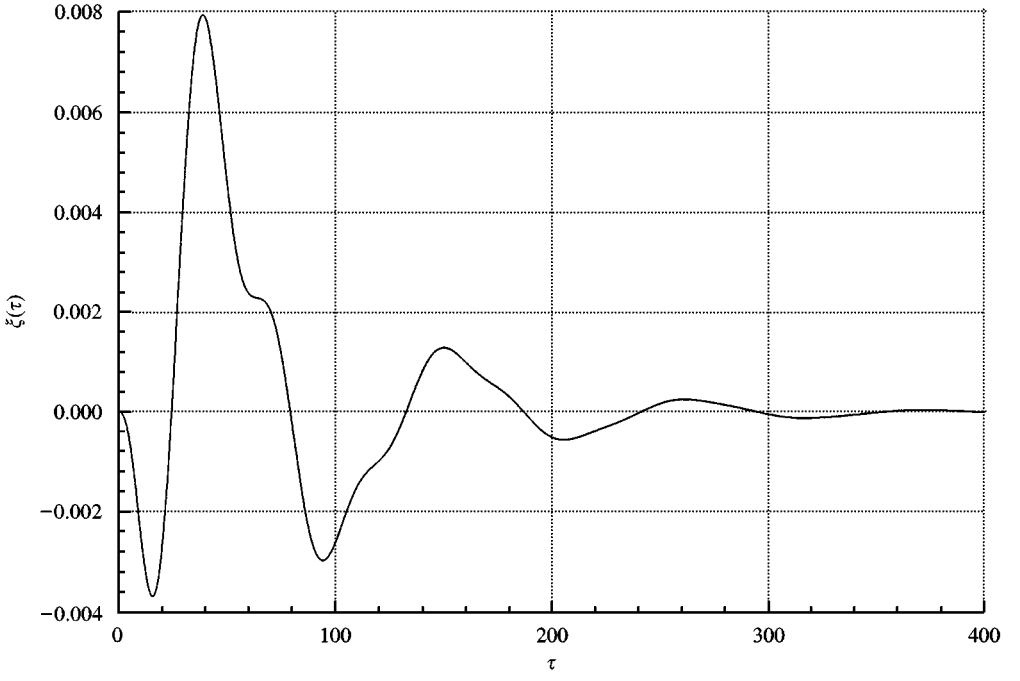

Figure 11. Time series of plunge motion at $U^*/U_L^* = 0.8$ with $\bar{\omega} = 0{\cdot}2$, $\mu = 100$, $a_h = -0.5$, $x_\alpha = 0{\cdot}25$, $r_\alpha = 0{\cdot}5$, $\zeta_\alpha = \zeta_\xi = 0$ and $\beta_\alpha = 3$.

Time series of ξ (Figure 11) show that for $U^*/U_L^* < 1$ more than one mode is present. We can write ξ as the sum of two modes as follows:

$$\xi = \sum_{n=1}^{2} \xi_{0n} e^{\lambda_n \tau}. \tag{53}$$

The two modes can be obtained by decomposing the time series using wavelets. The real and imaginary parts of λ can then be solved using equations (51) and (52) and their values are plotted in Figure 12 which shows fair agreement with the solution from the Jacobian matrix. It is difficult to obtain good accuracy of λ using equations (51) and (52) when only a few cycles of the time series are available. This is especially true for mode I which decays to practically zero values in less than three cycles. The results show the coalescence of the two modes, and after a short transient period, only mode II is present for $U^*/U_L > 1$. In the region of $0{\cdot}97 \leq U^*/U_L \leq 1$, the use of wavelets to separate the two modes becomes increasingly difficult as the two frequencies approach each other. Experience with wavelets (Lee & Wong 1998) shows that λ_r is difficult to obtain accurately when frequency separation between the two modes is not large.

In Figure 13 the eigenvalues of mode II for the pitch motion together with λ from numerical simulations shown in Figure 9 are replotted in the real and imaginary planes for $U^*/U_L^* = 0{\cdot}97$ to $1{\cdot}08$. The filled circle symbols denote numerical results, while the solid lines represent solutions from the eigenvalues of the Jacobian matrix. We can see that the real part of the complex conjugates increases with U^*/U_L^* and passes through zero at $U^*/U_L^* = 1{\cdot}0$ where a Hopf bifurcation occurs. With further increase in U^*/U_L^*, the real part of the conjugates switches sign and becomes positive, changing the stable equilibrium state to an unstable one.

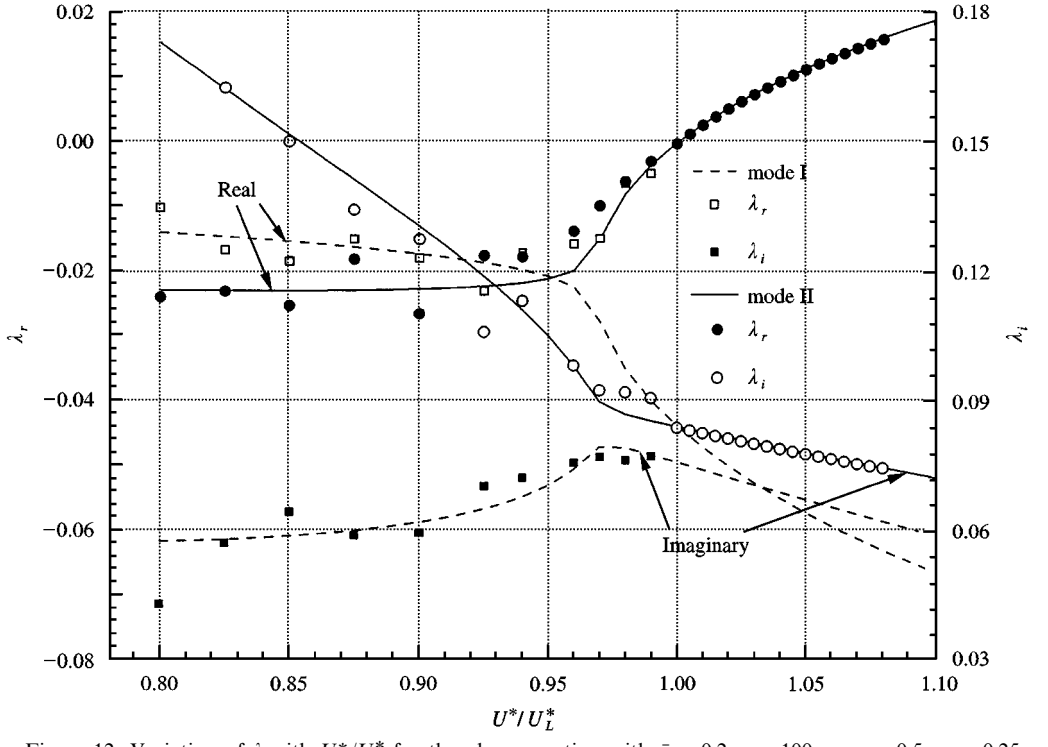

Figure 12. Variation of λ with U^*/U_L^* for the plunge motion with $\bar{\omega} = 0{\cdot}2$, $\mu = 100$, $a_h = -0.5$, $x_\alpha = 0{\cdot}25$, $r_\alpha = 0{\cdot}5$, $\zeta_\alpha = \zeta_\xi = 0$ and $\beta_\alpha = 3$.

3.4. Flutter Velocity and Angular Frequency at Hopf Bifurcation Point

By solving equation (34), we can determine the Hopf bifurcation point and find the linear flutter velocity and angular frequency at this point. These two quantities have been calculated for various parameters and compared with numerical simulation. The results show that, up to the fourth decimal point, there were no noticeable differences detected.

Figure 14 illustrates the variation of the linear flutter velocity and angular frequency at the Hopf point as functions of the frequency ratio $\bar{\omega}$ for $\mu = 100$, $x_\alpha = 0{\cdot}25$ and $r_\alpha = 0{\cdot}5$. The flutter velocity decreases with $\bar{\omega}$ until $\bar{\omega} = 0{\cdot}8$ is reached and increases from then on with increasing $\bar{\omega}$. The angular frequency increases rapidly with $\bar{\omega}$ initially until a maximum is reached at $\bar{\omega} = 1{\cdot}1$ and then decreases gradually. The effect of airfoil/air-mass ratio on flutter velocity and frequency shows the linear flutter velocity increases almost linearly with μ, while the frequency decreases monotonically. The effect of the distance between the centre of mass and the elastic axis shows that U_L^* decreases and ω increases with increases in x_α. The radius of gyration about the elastic axis has the effect of increasing the flutter velocity, while at the same time causes a decrease in frequency for increasing r_α.

3.5. Amplitude and Frequency of Limit-Cycle Oscillations

The amplitudes of pitch and plunge motion of LCO have been calculated for various values of U^*/U_L^*, using equations (48) and (50). The amplitudes of pitch and plunge motions are dependent on system parameters, velocity U^* and angular frequency ω of the LCO. In Figure 15, the angular frequency ω is plotted against U^*/U_L^* for $\bar{\omega} = 0{\cdot}2$, $\mu = 100$,

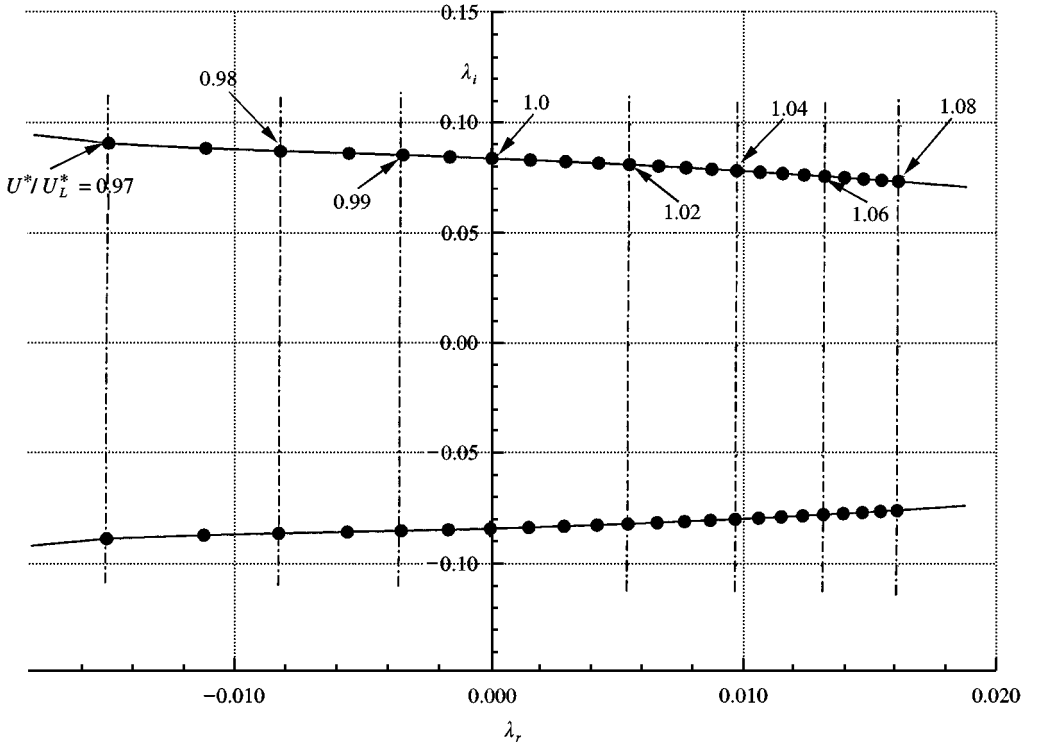

Figure 13. Variation of conjugate eigenvalues with U^*/U_L^* for pitch motion in the λ-plane for $\bar{\omega} = 0{\cdot}2$, $\mu = 100$, $a_h = -0.5$, $x_\alpha = 0{\cdot}25$, $r_\alpha = 0{\cdot}5$, $\zeta_\alpha = \zeta_\xi = 0$ and $\beta_\alpha = 3$.

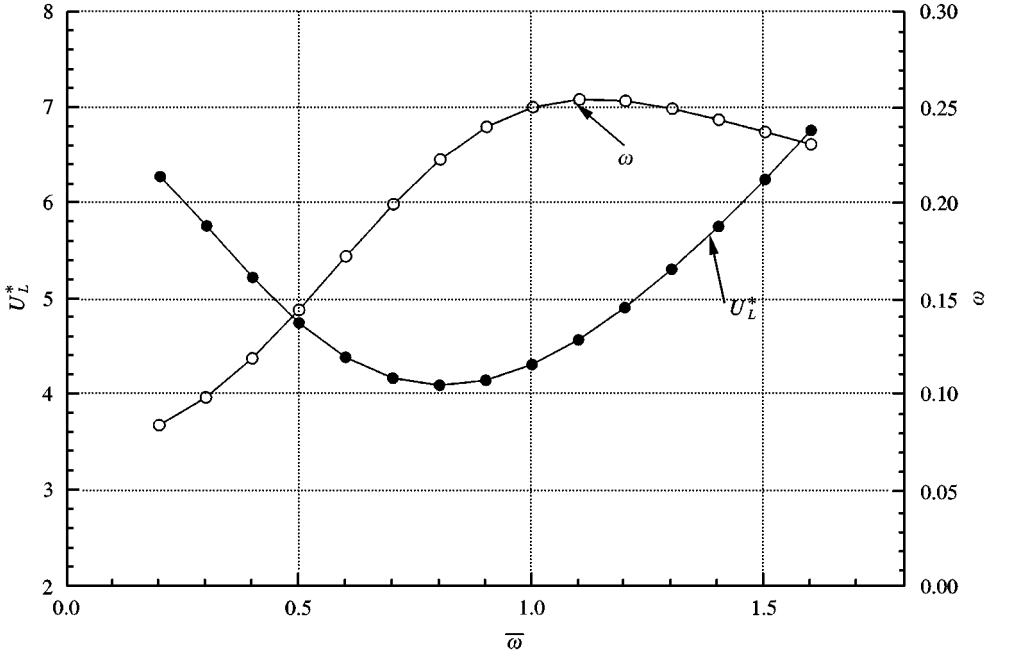

Figure 14. Variation of flutter velocity and frequency at the Hopf point for $\mu = 100$, $a_h = -0{\cdot}5$, $x_\alpha = 0{\cdot}25$, $r_\alpha = 0{\cdot}5$, and $\zeta_\alpha = \zeta_\xi = 0$.

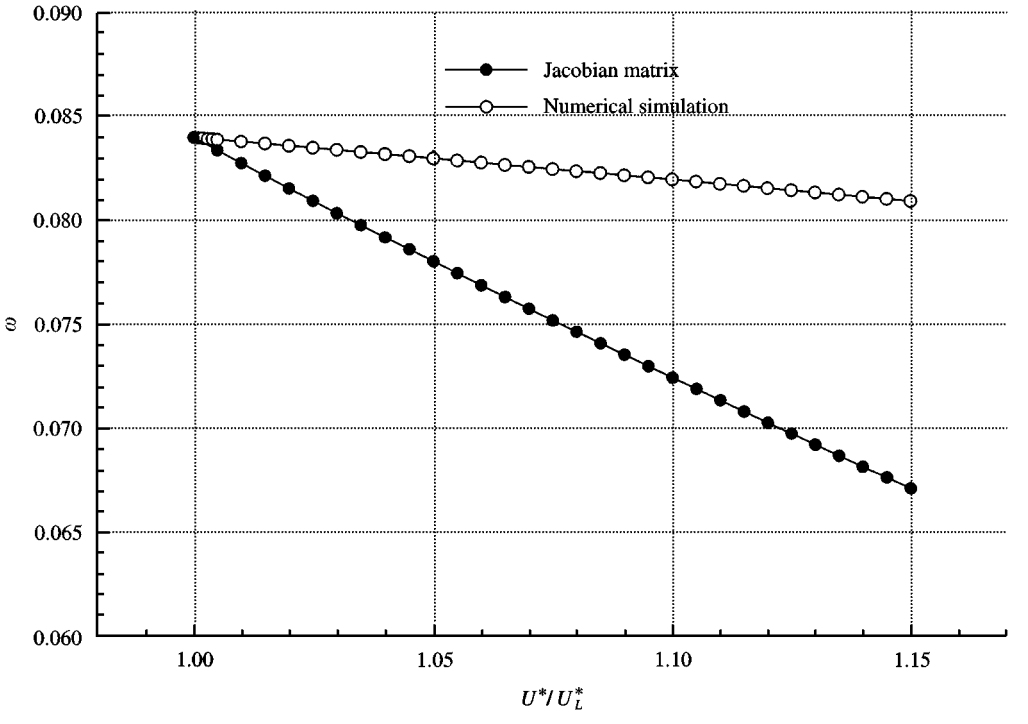

Figure 15. Variation of ω with U^*/U_L^* for pitch motion in the post-Hopf bifurcation range for $\bar{\omega} = 0{\cdot}2$, $\mu = 100$, $a_h = -0.5$, $x_\alpha = 0{\cdot}25$, $r_\alpha = 0{\cdot}5$, $\zeta_\alpha = \zeta_\xi = 0$ and $\beta_\alpha = 3$.

$x_\alpha = 0{\cdot}25$, $r_\alpha = 0{\cdot}5$ and $\beta_\alpha = 3$. The hollow symbol denotes ω obtained from numerical simulation using equation (15), while the solid symbols denote the value of the imaginary part of a pair of eigenvalues of the Jacobian matrix given in equation (21). The value of ω is small and the difference between the two frequency curves increases with increasing U^*/U_L^*. Results for $\bar{\omega} = 0{\cdot}8$ show the two frequency curves to be close to each other while the differences are again large for $\bar{\omega} = 1{\cdot}2$. The magnitudes of ω are similar in the latter two cases but are larger than those at the lowest $\bar{\omega}$ (for example, from numerical simulations, ω at $\bar{\omega} = 1{\cdot}2$ is 3·15 times that at $\bar{\omega} = 0{\cdot}2$ at $U^*/U_L^* = 1{\cdot}15$).

Figure 16 gives the amplitudes of pitch motion of LCO for various values of U^*/U_L^* at $\bar{\omega} = 0{\cdot}2$, $\mu = 100$, $x_\alpha = 0{\cdot}25$, $r_\alpha = 0{\cdot}5$ and $\beta_\alpha = 3$. The solid line is from numerical simulation, while the symbols are analytical results from equations (48) and (50). Three different angular frequencies are used to determine α_A. The solutions denoted by hollow circles are obtained using the frequency at $U^*/U_L^* = 1{\cdot}0$, and this frequency can be obtained from either numerical simulation or analytical method. The solid-circle results are calculated using the local frequency at a given U^*/U_L^* determined from numerical simulation. The solid triangle represents solutions obtained from the imaginary part of the conjugate eigenvalues of the Jacobian matrix. The amplitudes of pitch motion predicted by using various frequencies are in good agreement. For the other two values of $\bar{\omega}$ considered (that is, $\bar{\omega} = 0{\cdot}8$ and 1·2), it was found that using the frequency at $U^*/U_L^* = 1{\cdot}0$, the predicted results agree well with the numerical simulation for $\bar{\omega} = 1{\cdot}2$, but deviate from numerical solutions at $\bar{\omega} = 0{\cdot}8$. Using the imaginary part of the eigenvalues from the Jacobian matrix predicts the amplitudes of pitch angle of LCO for $\bar{\omega} = 0{\cdot}8$ fairly accurately, but fails to give acceptable results for $\bar{\omega} = 1{\cdot}2$.

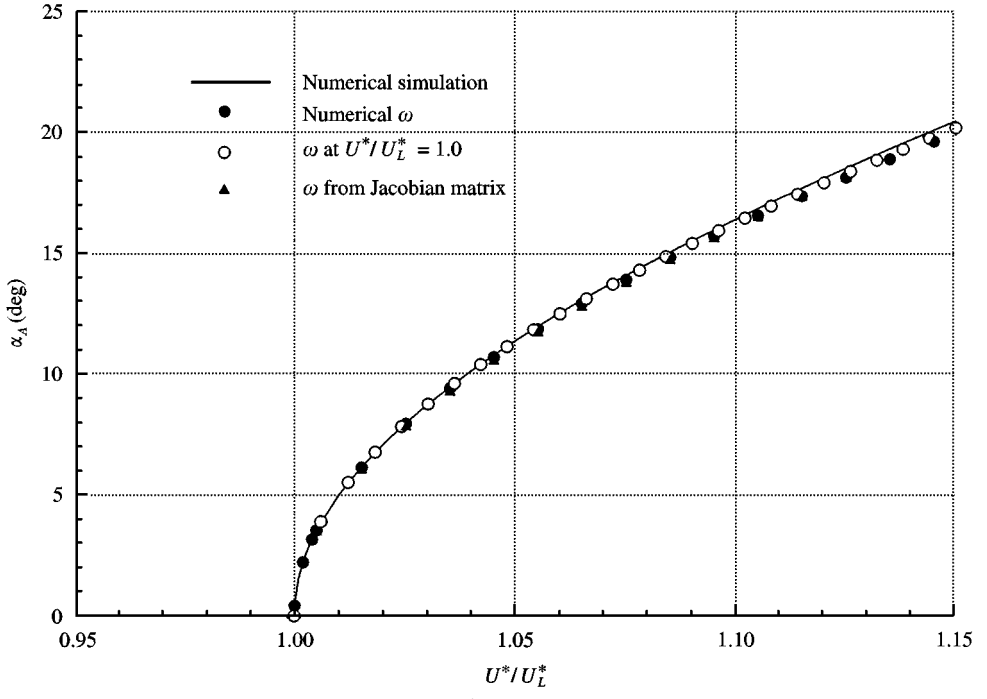

Figure 16. Variation of pitch amplitude with U^*/U_L^* in the post-Hopf-bifurcation range for $\bar{\omega} = 0{\cdot}2$, $\mu = 100$, $a_h = -0.5$, $x_\alpha = 0{\cdot}25$, $r_\alpha = 0{\cdot}5$, $\zeta_\alpha = \zeta_\xi = 0$ and $\beta_\alpha = 3$.

An explanation for the various agreements in pitch amplitude α_A using different ω can be seen from equation (50), which shows that α_A is given by R which contains terms of various powers of ω. For $\bar{\omega} = 0{\cdot}2$, ω is small and the differences in the values of ω obtained by various methods do not affect the magnitude appreciably. When $\bar{\omega} = 0{\cdot}8$ and $1{\cdot}2$, ω is much larger and has a greater effect on the amplitude α_A. The reason why the linear frequency gives good results at $\bar{\omega} = 1{\cdot}2$ is that the numerically determined ω values vary slightly with U^*/U_L^* and they are close to the linear value at $U^*/U_L^* = 1$. At $\bar{\omega} = 0{\cdot}8$, both numerical simulation and Jacobian matrix results are close, and the difference from the linear value is large. This accounts for the poor correlation between the numerically determined α_A and those obtained from equation (50) using the linear frequency at the Hopf point.

Figure 17 shows the amplitude of plunge motion ξ_A of LCO versus U^*/U_L^* for $\bar{\omega} = 0{\cdot}2$, $\mu = 100$, $x_\alpha = 0{\cdot}25$, $r_\alpha = 0{\cdot}5$ and $\beta_a = 3$. The results using the numerically determined values of ω and those with the linear frequency at the Hopf point agree reasonably well with numerical simulations. The agreement with the amplitudes determined using the frequencies from the Jacobian matrix becomes increasingly poorer as U^*/U_L^* moves further away from unity. It is shown in Figure 15 that the difference in frequencies between numerical and the Jacobian matrix solutions increases almost linearly with U^*/U_L^*. Unlike α_A , the plunge amplitude ξ_A is more sensitive to inaccuracies in ω.

4. CONCLUSIONS

Numerical simulations of the effect of a cubic structural restoring force in the pitch degree of freedom on the flutter characteristics of a two-dimensional airfoil placed in an incompressible flow have been carried out. The study shows the dependence of the divergence flutter boundary on initial conditions for a soft spring. For the spring constants and airfoil

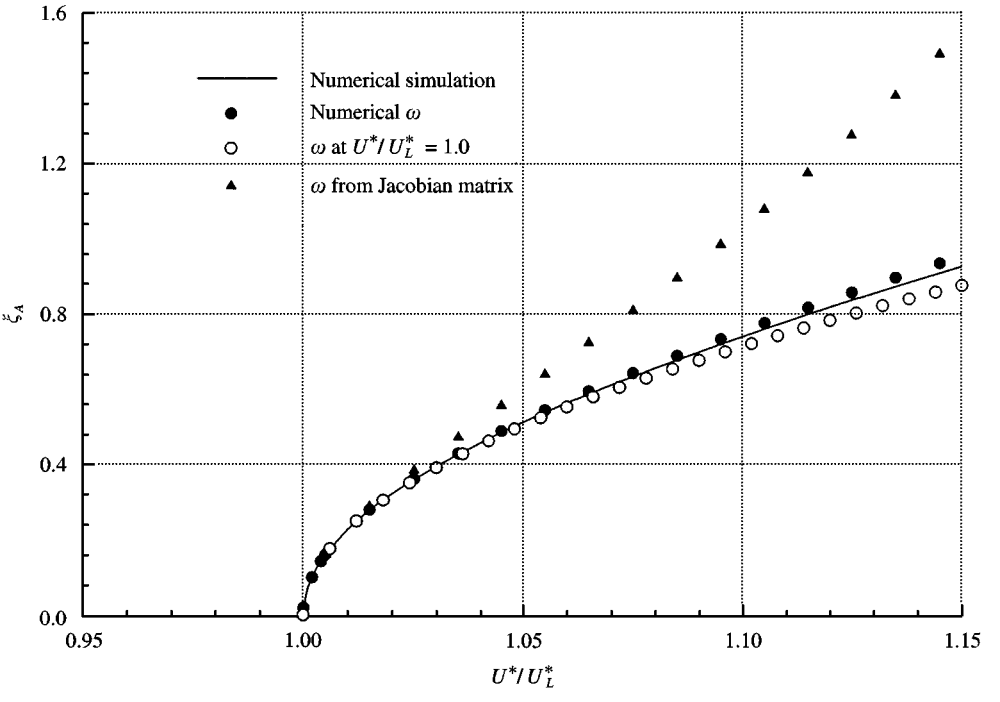

Figure 17. Variation of plunge amplitude with U^*/U_L^* in the post-Hopf-bifurcation range for $\bar{\omega} = 0{\cdot}2$, $\mu = 100$, $a_h = -0.5$, $x_\alpha = 0{\cdot}25$, $r_\alpha = 0{\cdot}5$, $\zeta_\alpha = \zeta_\xi = 0$ and $\beta_\alpha = 3$.

parameters investigated, the flutter speed decreases with increasing values of the initial pitch and plunge displacements and their velocities. A hard spring, on the other hand, has a flutter boundary that is independent of initial conditions. The nonlinear flutter speed coincides with the linear flutter speed. Divergent flutter is not encountered, but instead limit-cycle oscillation is observed for velocities greater than the flutter speed. At the flutter speed, a supercritical Hopf bifurcation occurs.

In the post-Hopf bifurcation range, for a hard spring, the frequency of the LCO is evaluated using an approximate method. For the airfoil parameters chosen in this study, agreement with numerical simulations is affected only by the plunge to pitch natural frequency ratio. The amplitude of the LCO as a function of the frequency is predicted using an asymptotic theory. The results compare favourably with numerical solutions for small values of the limit-cycle frequency since in such cases the amplitude is weakly dependent on the frequency. For larger values of the frequency, the agreement deteriorates. The method used to determine the frequency of the limit-cycle oscillation is valid only in the region close to the Hopf point (i.e. $U^*/U_L^* = 1$). This deficiency in the present analysis can be eliminated by a more mathematical study using the centre manifold theory and the principle of normal forms. Some preliminary investigation shows that the equations can be reduced to a single ordinary differential equation, and a frequency relationship can be determined for given airfoil parameters.

ACKNOWLEDGEMENTS

The authors gratefully acknowledge the financial support from the Natural Sciences and Engineering Research Council of Canada.

References

Arnold, V. I. 1980 *Ordinary Differential Equations*. Cambridge, MA: The MIT Press.

Dowel, E. H. & Ilgamov, M. 1988 *Studies in Nonlinear Aeroelasticity*. New York: Springer-Verlag.

Fung, Y. C. 1969 *An Introduction to the Theory of Aeroelasticity*. New York: Dover Publications.

Gong, L., Wong, Y. S. & Lee, B. H. K. 1998 Dynamics of a coupled system of Duffing's equations. In *Dynamics of Continuous, Discrete and Impulsive Systems*, volume 4, pp. 99–119.

Hayashi, C. 1964 *Nonlinear Oscillations in Physical Systems*. New York: McGraw-Hill.

Houbolt, J. C. 1950 A recurrence matrix solution for the dynamic response of elastic aircraft. *Journal of the Aeronautical Sciences* **17,** 540–550.

Johnson, E. C. 1952 Sinusoidal analysis of feedback-control systems containing nonlinear elements. *Transaction of AIEE* **71,** 169–181.

Jones, D. J. & Lee, B. H. K. 1985 Time marching numerical solution of the dynamic response of nonlinear systems. Aeronautical Note NAE-AN-25, NRC No. 24131, *National Research Council of Canada*.

Jones, R. T. 1940 The unsteady lift of a wing of finite aspect ratio. Report 681. *NACA*.

Jordan, D. W. & Smith, P. 1983 *Nonlinear Ordinary Differential Equations*. Oxford: Clarendon Press.

Lee, B. H. K. & Leblanc, P. 1986 Flutter analysis of a two-dimensional airfoil with cubic nonlinear restoring force. Aeronautical Note NAE-AN-36, NRC No. 25438, *National Research Council of Canada*.

Lee, B. H. K. & Desrochers, J. 1987 Flutter analysis of a two-dimensional airfoil containing structural nonlinearities. Aeronautical Report LR-618, NRC No. 27833, *National Research Council of Canada*.

Lee, B. H. K., Gong, L. & Wong, Y. S. 1997 Analysis and computation of nonlinear dynamic response of a two-degree-of-freedom system and its application in aeroelasticity. *Journal of Fluids and Structures* **11,** 225–246.

Lee, B. H. K. & Wong, Y. S. 1998 Neural network parameter extraction with application to flutter signals. *Journal of Aircraft* **35,** 165–168.

Lee, B. H. K., Jiang, L. Y. & Wong, Y. S. 1998 Flutter of an airfoil with a cubic nonlinear restoring force. AIAA Paper 98–1725.

Morton, S. A. & Beran, P. S. 1996 Hopf-bifurcation analysis of airfoil flutter at transonic speeds. AIAA paper 96–0060.

O'neil, T., Gilliatt, H. & Strganac, T. 1996 Investigation of aeroelastic response for a system with continuous structural nonlinearities. AIAA paper 96–1390.

Poirion, F. 1993 Effects of structural nonlinearities on flutter analysis. In *Proceedings of Forum International l'Aéroélasticité et Dynamique de Structures*, Strasbourg, Vol. 2, pp. 857–869.

Price, S. J., Alighanbari, H. & Lee, B. H. K. 1995 The aeroelastic response of a two-dimensional airfoil with bilinear and cubic structural nonlinearities. *Journal of Fluids and Structures* **9,** 175–193.

Seydel, R. 1988 *From Equilibrium to Chaos*. New York: Elsevier.

Stoker, J. J. 1950 *Nonlinear Vibrations in Mechanical and Electrical Systems*. New York: Interscience Publishers.

Thompson, J. M. T. & Stewart, H. B. 1986 *Nonlinear Dynamics and Chaos*. Chichester, U.K., John Wiley.

Ueda, Y. 1980 Steady motions exhibited by Duffing's equation: a picture book of regular and chaotic motions. In *New Approaches to Nonlinear Problems in Dynamics* (ed. P. J. Holmes), pp. 311–322. Philadelphia: SIAM.

Wiggins, S. 1990 *Introduction to Applied Nonlinear Dynamical Systems and Chaos*. New York: Springer-Verlag.

Wong, Y. S. Lee, B. H. K. & Gong, L. 1995 Dynamic response of a two-degree-of-freedom system with a cubic nonlinearity. *Third International Conference on Computational Physics*, Chung Li, Taiwan.

Woolston, D. S., Runyan, H. L. & Byrdsong, T. A. 1995 Some effects of system nonlinearities in the problem of aircraft flutter. NACA TN 3539.

Woolston, D. S. Runyan, H. L. & Andrews, R. E. 1957 An investigation of effects of certain types of structural nonlinearities on wing and control surface flutter. *Journal of Aeronautical Sciences* **24,** 57–63.

Zhao, L. C. & Yang, Z. C. 1990 Chaotic motions of an airfoil with nonlinear stiffness in incompressible flow. *Journal of Sound and Vibration* **138,** 245–254.

APPENDIX: NOMENCLATURE

a_h	nondimensional distance from airfoil mid-chord to elastic axis
b	airfoil semi-chord
C_L	aerodynamic lift coefficient
C_M	pitching moment coefficient
h	plunge displacement
m	airfoil mass
R	response amplitude of pitch motion
r	response amplitude of plunge motion
r_α	radius of gyration about elastic axis
t	time
U	free stream velocity
U^*	nondimensional velocity, $U/b\omega_\alpha$
U_L^*	nondimensional linear flutter speed
x_α	nondimensional distance from elastic axis to centre of mass
$\mathbf{X}$	system variable vector
$\mathbf{X}_E$	system equilibrium point
$\mathbf{y}$	variable vector
α	pitch angle of airfoil
α_A	pitch angle amplitude of limit-cycle oscillation
β_α, β_ξ	coefficients of cubic spring in pitch and plunge
$\varepsilon_1, \varepsilon_2$	constants in Wagner's function
ζ_α, ζ_ξ	viscous damping ratios in pitch and plunge
λ	eigenvalue
μ	airfoil/air mass ratio, $m/\pi\rho b^2$
ξ	nondimensional plunge displacement, h/b
ξ_A	plunge amplitude of limit-cycle oscillation
τ	nondimensional time Ut/b
ϕ	Wagner's function
ψ_1, ψ_2	constants in Wagner's function
ω	frequency
$\omega_\alpha, \omega_\xi$	natural frequencies in pitch and heave
$\bar{\omega}$	frequency ratio, ω_ξ/ω_α